JOURNAL OF GEOPHYSICAL RESEARCH, VOL. 102, NO. B3, PAGES 5327-5352, MARCH 10, 1997

# Gravity anomalies and spatial variations of flexural rigidity at mountain ranges

J. Stewart and A. B. Watts
Department of Earth Sciences, University of Oxford, Oxford, England

**Abstract.** New continent-wide compilations of gravity and topography data have been used to determine spatial variations in the long-term mechanical properties of the foreland lithosphere at mountain ranges. In the southern Appalachians, a large elastic thickness $T_e$ (in the range 40-70 km) is required with variation only along the length of the mountain range. To explain the Appalachian Bouguer gravity anomaly "high", a subsurface load and crustal thinning are necessary. For the Andes, $T_e$ varies in the range 5-85 km perpendicular and parallel to the length of the mountain range. In the Alps, $T_e$ is high in the French Alps and then decreases in the western Swiss Alps and increases toward the eastern Alps. In the Romanian Carpathians, $T_e$ variations in the range 5-20 km are found. Although the thermal state, curvature, and inelastic yielding may play some role, these variations in $T_e$ are interpreted as the result of inheritance of the thermal and mechanical properties of foreland lithosphere. Inheritance plays a role in influencing the development of the next plate tectonic event. At mountain ranges, preexisting strength variations offer some control on tectonic style, the geometry of fold and thrust belts, and the stratigraphic patterns that develop in the adjacent foreland basin. Foreland lithosphere is involved in a cycle of events that began with continental rifting and passive margin formation and ended in continental collision. Compilations of $T_e$ from continental rifts, passive margins, and foreland lithosphere show large variations. The lowest values are associated with rifts, margins, and foreland lithosphere which has recently been been involved in continental breakup. The highest values are associated with foreland lithosphere for which a long time has elapsed since the previous rifting event. We speculate that continental lithosphere undergoes some form of strength recovery.

## Introduction

The lithosphere's response to long-term ($> 10^6$ years) geological loads has been successfully modeled as a thin elastic plate of thickness $T_e$ overlying a weak fluid substratum. This model has been used extensively in the oceans [e.g., *Walcott*, 1970; *Watts and Cochran*, 1974] and continents [e.g., *Karner and Watts*, 1983; *Lyon-Caen and Molnar*, 1983]. In the oceans, variation of $T_e$ can be explained by a simple secular cooling model, with the thickness given approximately by the depth to the 450°C isotherm [*Watts*, 1978]. However, in the continents the exact physical meaning of $T_e$ is unclear, and a number of properties are important in its control. These include the thermal state, the proportions of crustal and mantle strength, crustal composition and thickness, the local curvature, and in-plane stresses [*Burov and Diament*, 1995]. Despite this, $T_e$ is an extremely useful measure of the integrated strength of the lithosphere which can be compared from region to region and interpreted in terms of the thermal and mechanical structure of the continental lithosphere.

Maps of elastic thickness (e.g., *Zuber et al.* [1989] of Australia, *Bechtel et al.* [1990] of North America, *Lowry and Smith* [1994] of the Basin and Range area, and *Hartley et al.* [1996] of Africa) show large variations. Cratonic areas appear flexurally strong, and tectonically active areas and rifts appear flexurally weak. Some of the lowest values of $T_e$ have been observed at passive margins [*Barton and Wood*, 1984; *Watts*, 1988; *Fowler and McKenzie*, 1989] despite the fact that rifting occurred at some of these margins in the Mesozoic. The reason why stretched continental lithosphere should remain weak for such long periods of time after rifting is controversial as other workers [e.g., *Kooi et al.*, 1992] suggest that rifted margins do possess some significant strength. Irrespective of whether stretched continental lithosphere is fundamentally weak, lateral variations in $T_e$ are expected to exist as we move from margins toward the interior of continents.



Paper number 96JB03664.
0148-0227/97/96JB-03664$09.00

According to plate tectonic models [e.g., *Dewey*, 1982; *Tankard*, 1986; *Stockmal et al.*, 1986], thrust/fold belts advance across former passive margins onto more cratonic lithosphere. They therefore sample a gradient of $T_e$, and this would be expected to exert a strong influence on the geometry of the foreland basin that forms by flexure in front of the load and its stratigraphic fill. For example, some foreland basins are deep and narrow (e.g., Apennines) and others are wide and shallow (e.g., Ganges) which *Watts* [1992] related to their formation on stretched and unstretched lithosphere, respectively. He also showed that for lateral variations in $T_e$ and simply evolving load geometries, the shape of the foreland basin and the stratigraphy developed strongly reflect the properties of the lithosphere on which these basins develop. More recently, *Watts et al.* [1995] inferred variations in $T_e$ of the Brazilian shield which underthrusts the South American Andes and related changes in the tectonic style of deformation in the orogen to these variations in strength.

Previous studies of continent-wide gravity and topography data have used spectral techniques such as admittance or coherence to estimate $T_e$ [*Dorman and Lewis*, 1970; *McNutt and Parker*, 1978; *Zuber et al.*, 1989; *Bechtel et al.*, 1990; *Hartley et al.*, 1996]. By their very nature these methods provide only an average estimate of $T_e$ for a region, and this prevents a detailed analysis of the spatial variation of $T_e$ within a region. Admittance is biased toward low values of $T_e$ if a number of different strength regions are combined since it places most emphasis on those regions with the greatest topographic relief [*Forsyth*, 1985]. Coherence is biased if surface and subsurface loads are correlated [*Macario et al.*, 1995] as is the case in many geological settings such as mountain belts, seamounts, and underplated sedimented passive margins. Both methods are biased if the size of the area is too small to fully resolve the $T_e$.

A preferred approach is to forward model the gravity data. However, a sparsity of high-quality data has limited forward modeling to studies of a few widely spaced profiles [e.g., *Karner and Watts*, 1983; *Lyon-Caen and Molnar*, 1983; *Caporali*, 1995], and the estimates of $T_e$ obtained have tended to refer to the mountain belt as a whole rather than to variations along it. Recently, several continent-wide compilations of high-quality gravity anomaly and topography data have become available for South America, western Europe, North America, and Africa. Therefore it may now be possible to recover the along-strike variations in the mechanical properties of the continental lithosphere.

The purpose of this paper is to use a forward modeling approach to systematically estimate $T_e$ of the foreland lithosphere at mountain ranges of widely differing ages and spatial distribution. In particular, we shall determine how the integrated strength of the continental lithosphere varies along the length of a mountain range. These variations in strength are interpreted in terms of the thermal and mechanical structure of the continental lithosphere which is a function of its tectonic evolution. The influence of these variations is examined in relation to (1) the types of deformation in fold/thrust belts and (2) the geometry and stratigraphy of foreland basins.

## Data

For North America the Decade of North American Geology (DNAG) data set released in 1989 is used. The gravity (Bouguer on land and free-air offshore) data set is based on about $1\text{x}10^6$ land and $0.8\text{x}10^6$ marine gravity values from the Defense Mapping Agency (DMA) and other academic and commercial sources. It is provided as a 4 km grid.

For South America gravity anomaly and topography data compiled by GETECH as part of its South American Gravity Project (SAGP) [*Green and Fairhead*, 1991] are used. The data consisted of over 300,000 2.5 arc min by 2.5 arc min marine and land-corrected smoothed values. Coverage is poor in the Amazon Basin, parts of the high Andes, and southern Chile and Argentina. In addition a 3 arc min by 3 arc min Digital Terrain Model (DTM) from GETECH enables a comparison with the SAGP topographic data to be made and poor quality profiles to be rejected.

For western Europe a prerelease corrected 8 km grid of gravity and a 4 km grid of topography compiled by GETECH as part of its Western Europe Gravity Project (WEEGP) are used. Over $2.3\text{x}10^6$ land, marine, and satellite measurements were used in the construction of this grid. Coverage is excellent apart from Greenland, Turkey, and parts of the Balkans.

The standard corrections and adjustments were applied to the gravity data sets. These include base-station tie in errors, intersurvey compatibility, and removal of outliers. Terrain corrections out to 166.67 km were applied and crossover analysis was applied to marine values [*Wessel and Watts*, 1988]. The data were adjusted to the 1971 International Gravity Standardization Network and reduced to free-air gravity anomalies using the 1967 International Gravity Formula. Bouguer anomalies were calculated using a density of 2670 kg $m^{-3}$ on land.

Where necessary, a conversion from the kilometer grid format to a longitude-latitude format is performed, and then these "point" measurements are smoothed over 2.5 arc min or 5 arc min squares depending on the resolution of the original data before gridding on a 5 arc min by 5 arc min grid using a curvature spline in tension technique [*Smith and Wessel*, 1990].

We remove up to and including degree and order 16 gravity field from the continent-wide data sets as calculated by the global geopotential model, OSU91a [*Rapp et al.*, 1991] in order to isolate contributions from below the lithosphere. For example, there is a

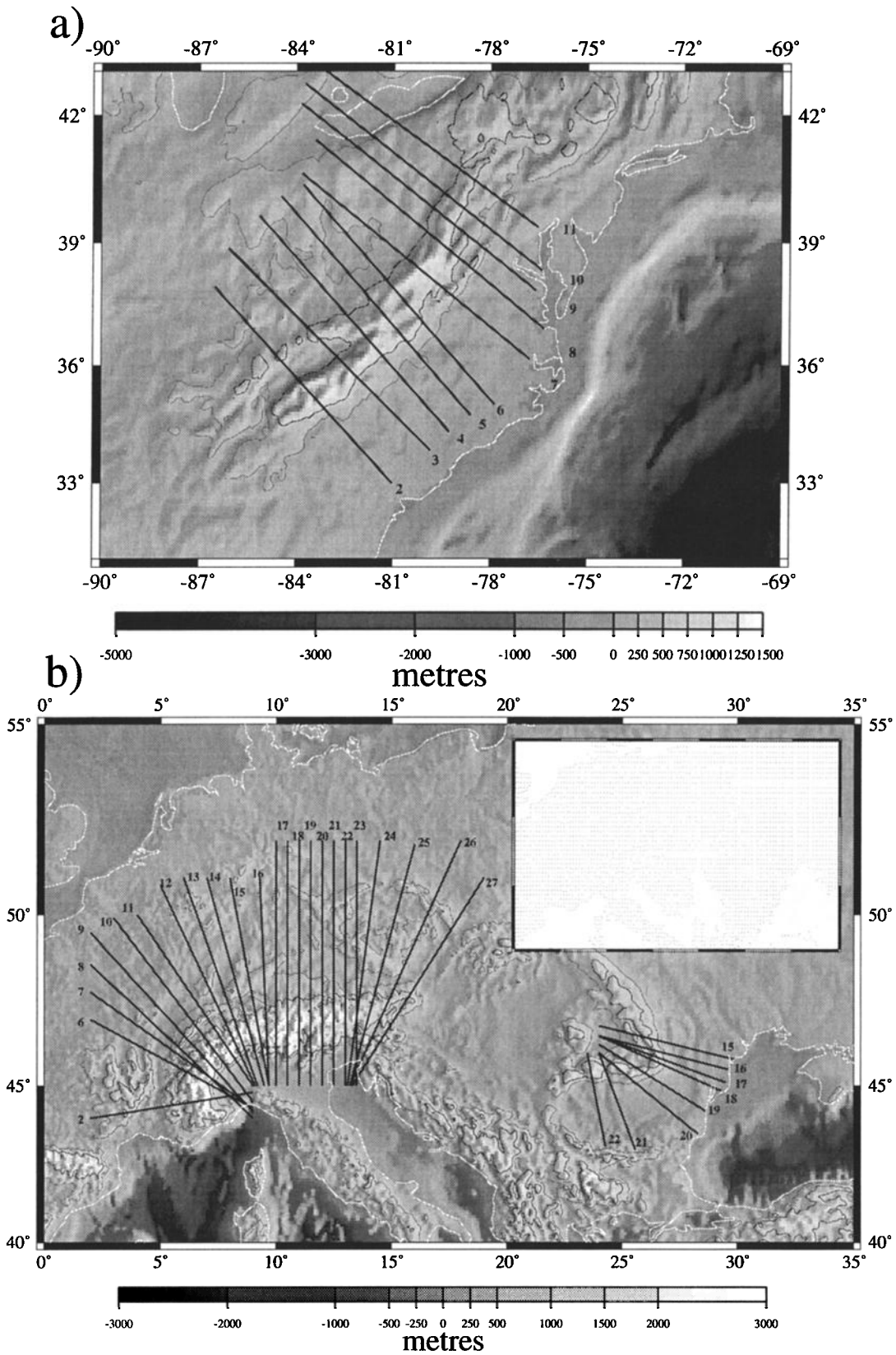


**Figure 1.** (a) Shaded relief map of North East America from Decade of North American Geology (DNAG) data set with locations of profiles. Topography is illuminated from the northwest. The 250 m and 500 m contour are shown. (b) Shaded relief map of central Europe from Western Europe Gravity Project (WEEGP) data set with locations of profiles. Topography is illuminated from the west. The 500 m and 1000 m contour are shown. Inset shows location of 20 arc min x 20 arc min data bins with at least one data measurement.

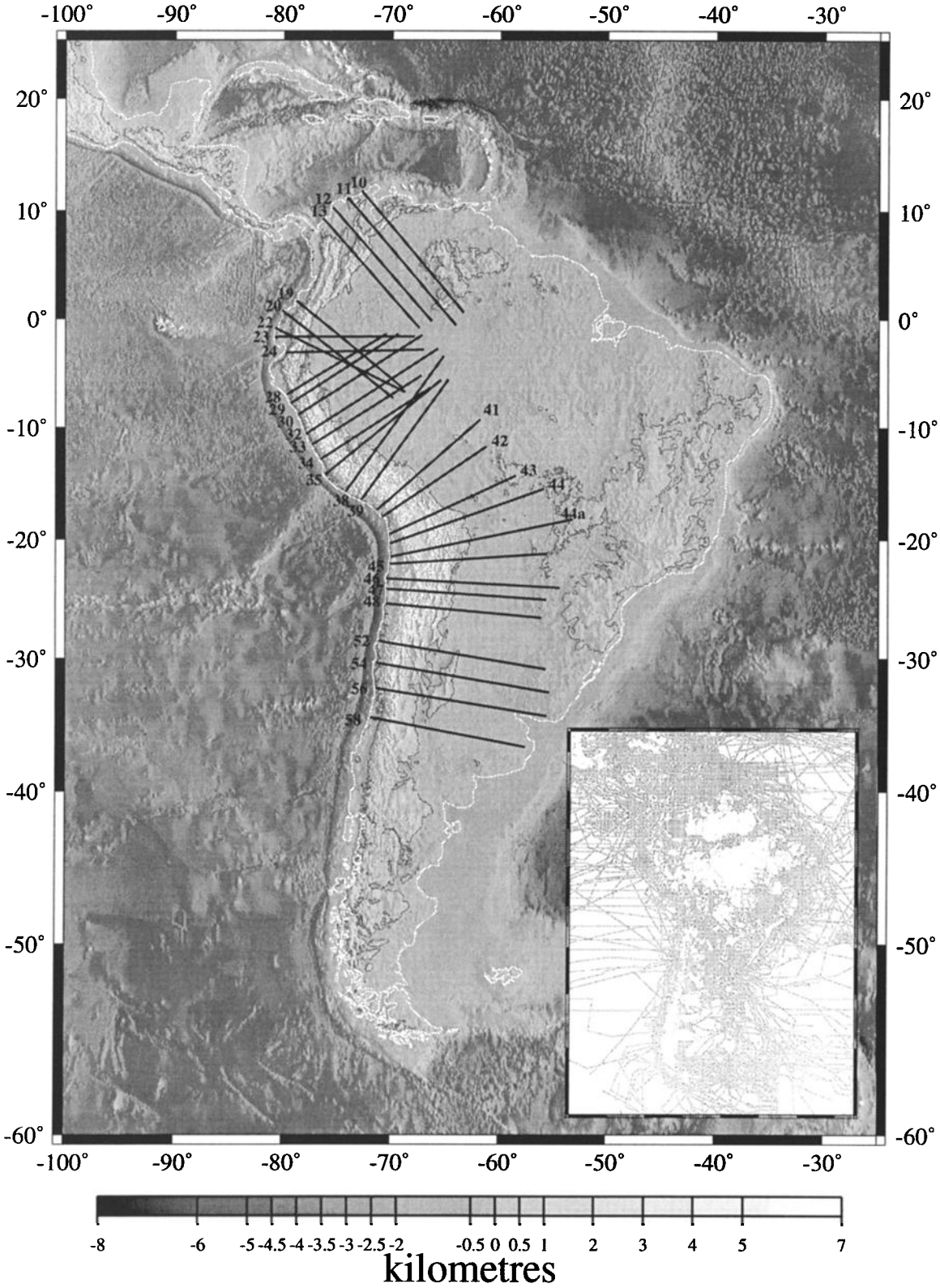


**Figure 2.** Shaded relief map of South America from GETECH DTM3 with locations of profiles. Topography is illuminated from the west. The 1000 m contour is shown. Inset shows 20 arc min x 20 arc min data bins with at least one measurement of gravity.

long-wavelength, high-amplitude positive anomaly associated with the Pacific rim, and this is thought to be related to subducting slabs [*Kaula*, 1969]. The resulting anomalies resolve features in the gravity field with wavelengths less than about 2500 km.

We extract profiles from these gridded data sets along great circle tracks with 10 km spacing between points. We reject those profiles where coverage is poor by considering, where appropriate, the distribution of point measurements within 25 km of the track. Figures 1 and 2 show the location of the profiles. The insets, where appropriate, give locations of all 20 arc min by 20 arc min data bins with at least one observation.

## Model

The first stage of the model is to assume that the observed surface topography $h$ is supported by an Airy-type model of crustal thickening, with the thickness of the root, $t_{root}$, given by

$$t_{root} = \frac{\rho_c}{(\rho_m - \rho_c)} h \quad (1)$$

where $\rho_c$ and $\rho_m$ are the densities of the crust and mantle (given in Table 1). Gravity anomalies arising from this root are calculated using the fast Fourier transform method of *Parker* [1972](see the appendix).

**Table 1.** List of Physical Parameters

| Parameter | Definition | Value |
|---|---|---|
| $E$ | Young's modulus | $1 \times 10^{11}$ N m |
| $\nu$ | Poisson's ratio | 0.25 |
| $g$ | gravitational acceleration | 9.81 m $s^{-2}$ |
| $\rho_c$ | density of crust | 2670 kg $m^{-3}$ |
| $\rho_m$ | density of mantle | 3300 kg $m^{-3}$ |

Figure 3 shows a typical observed Bouguer anomaly and a calculated gravity anomaly assuming Airy isostasy for each of the three mountain belts. By considering the difference between the observed and calculated anomalies (i.e., the isostatic anomaly), we propose that the Bouguer anomaly is better explained by a regional type isostatic mechanism rather than a local mechanism. The methods used to solve the flexure equation are presented in the appendix.

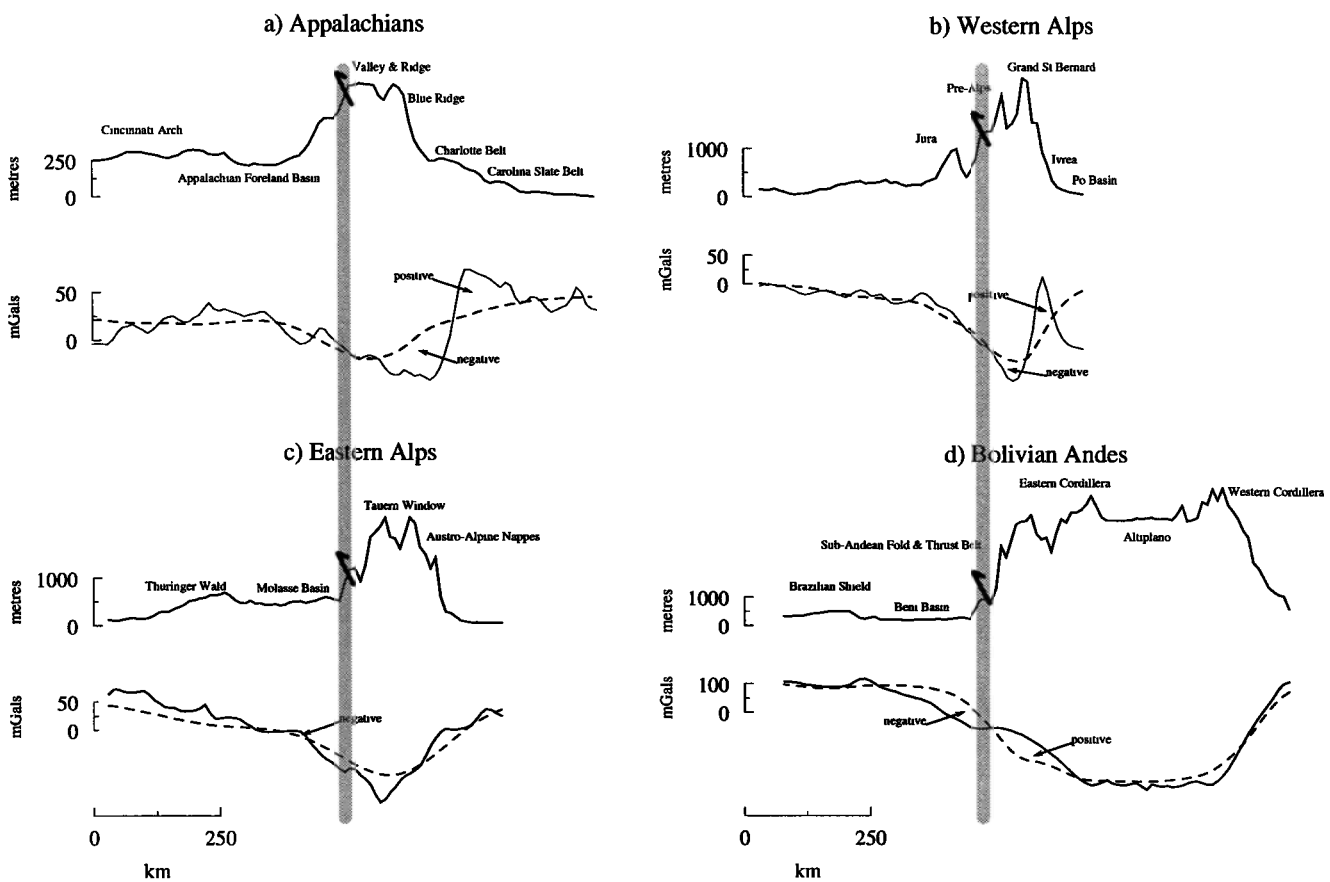


**Figure 3.** Typical profiles of (top) topography and (bottom) gravity for (a) Appalachians, (b) Western Alps, (c) Eastern Alps and (d) Andes, stacked on the position of the outermost thrust (thick grey line and schematic thrust symbol). For the gravity profiles, the solid line is the observed Bouguer anomaly and the dashed line is the gravity anomaly calculated assuming Airy isostasy. Note Andean profile is reversed relative to later figures.

Figure 3a shows a typical profile of topography and gravity from the southern Appalachians with the gravity anomaly calculated assuming an Airy compensation of topography. An obvious positive/negative pair of isostatic anomalies exist. There is evidence for crustal thickness variations across this gravity anomaly pair from teleseismic analysis and regional seismic lines (see references of *Taylor* [1989]). *Hutchinson et al.* [1983] show that this variation contributes significantly to the observed anomaly pair with crustal thickening explaining the gravity low and a marked decrease in crustal thickness explaining the gradient and much of the amplitude of the gravity high. We propose that the origin of the crustal thickening is a result of flexure of the foreland lithosphere under the loads of topography (surface load) and overthrust blocks (subsurface load). We model the flexure using a semi-infinite or broken plate model. The plate break is assumed to be at the position of the eastern edge of the positive isostatic anomaly. The location of these extra subsurface loads (e.g., the Carolina Slate Belt) explains why the negative isostatic anomaly (and crustal thickening) is displaced to the south east of the topographic high of the Valley and Ridge province. We model these overthrust loads by assuming that beneath the gravity high the density of the infilling material is 2850 kg $m^{-3}$, typical for overthrust material of a middle crustal origin. The extra density of the overthrust load explains the remainder of the gravity high. Toward the foreland, infill density decreases to 2500 kg $m^{-3}$, more typical of sediments of the foreland basin.

We therefore incorporate crustal thinning into our model to explain the gradient and part of the amplitude of the gravity high. Thinning of the crust at depth must be balanced isostatically with subsidence in the upper crust. We assume that this subsidence is Airy type but note that this may be inappropriate [*Kooi et al.*, 1992]. The subsidence results in the formation of a water-filled depression (i.e., paleobathymetry) which thrust loads can infill. The displacement of water by the thrust material provides an extra load which *Stockmal et al.* [1986] offer as an explanation of the additional shear forces required in previous models [e.g., *Karner and Watts*, 1983; *Nunn et al.*, 1987].

Overthrusting of extended and thinned foreland lithosphere is consistent with the geological history of the Appalachians [e.g., *Hatcher*, 1989] and seismic reflection profile data. Deviations between observed and calculated Bouguer anomalies at the north west end of the profile in Figure 3a arise as a result of the compensation of the interior U.S. basins.

For profiles in the western Alps (up to profile 13 on Figure 1b) we use the same method as for southern Appalachians as a typical profile (Figure 3b) shows the same sense of positive and negative isostatic anomalies. These profiles cut across ultramafic rocks exposed at the surface, e.g., at Lanzo and Ivrea. These bodies are a major subsurface load, and we assume an infill density for the subsurface load of 3100 kg $m^{-3}$, typical of overthrust obducted material of oceanic affinity beneath the gravity high. The infill density outboard of the subsurface load is 2500 kg $m^{-3}$. As in the Appalachian analysis, the break is defined at the southern end of the positive isostatic anomaly which we believe marks the trailing edge of the thrust loads.

Figures 3c and 3d show profiles of observed and calculated Airy gravity anomalies from the eastern Alps and Bolivian Andes. Figure 3d shows an obvious pair of positive and negative Airy isostatic anomalies but of reversed sense to those in the southern Appalachians and western Alps. This pair can most easily be interpreted as a result of flexural support of the surface topographic load. Support of topography is reduced beneath the mountain range and transferred toward the foreland by the strength of the plate. This increases the calculated gravity anomaly beneath the high topography and decreases the calculated anomaly beneath the foreland. We model these profiles using a broken elastic plate model with the break occurring where the Bouguer anomaly flattens off and begins to coincide with the calculated gravity anomaly assuming local compensation. In the Andes this is approximately beneath the western edge of the Eastern Cordillera and its along-strike continuations. The infill density was fixed at 2670 kg $m^{-3}$ as the exact locations of the sub-Andean foreland basins are poorly known.

On the Andean profile, because the observed and calculated anomalies agree beneath the load, it seems that the topographic load is sufficient, and it is not necessary to apply subsurface loads. However, on some profiles from the Andes and eastern Alps (e.g., as on Figure 3c) calculated and observed gravity anomalies do not agree beneath the maximum topographic load, and so in these cases an additional shear force is applied at the end of the plate.

We have modeled the profiles using a broken plate flexural model. First, the observed gravity anomalies are distinctly asymmetric and this suggests the use of a broken plate rather than a continuous one. Second, our modeling approach is process orientated, and it seems more likely for overthrust material to be emplaced onto an upper surface of a subducted plate of limited length. Third, the position of the plate break in the Alps corresponds to the major structural sutures of the Insubric Line and its along-strike continuations. Fourth, there are examples in the Andes where the position of the break corresponds to the point where the observed Bouguer anomaly begins to agree with the calculated gravity anomaly assuming Airy isostasy. In the case of the Appalachians, even though a long time has elapsed since the end of orogeny, which might have healed a break, we do not mean to imply that later loads on the North American lithosphere would load a broken plate. On the mountainward side of the plate break, we assume that in all cases topography is supported by crustal thickening. No attempt is therefore made to

model the observed Bouguer anomaly in these regions.

In reality, there may be some coupling between each side of the break, and this may offer an origin for the additional shear forces that are required in our modeling of the Alps and Andes. An alternative origin for the shear force may be related to subsurface loads such as igneous intrusions. In the Andes the shear forces may result from mantle dynamics related to corner flow in the mantle wedge as proposed by *Toth et al.* [1996]. The values of the other constant parameters used are shown in Table 1.

## Results

To find the best set of parameters, it is necessary to minimize the difference between observed and calculated data. Usually, this is expressed in the least squares sense as the rms residual. The least squares method, however, can give too much emphasis to short-wavelength, large-amplitude misfits at the expense of the long wavelengths which are of importance to flexure studies. We therefore use the correlation coefficient $r$ in addition, and our objective is to minimize the rms residual and maximise $r$ using a trial and error method.

### Appalachians

Figure 1a shows the location of the 10 profiles studied each of which was orientated perpendicular to the local strike of the mountain range. $T_e$ and the amount of crustal thinning are constrained by minimizing the difference between observed and calculated gravity anomalies and the additional constraint provided by the depth to the base of the Appalachian foreland basin, constructed from Paleozoic isopach maps of *Milici and de Witt* [1988]. Figure 4 shows the best fit $T_e$ and range of possible $T_e$ for the profiles studied and the amount of crustal material removed by thinning for the best $T_e$.

A typical crustal structure output from the model and the gravity anomalies associated with it are shown in Figure 5. A subsurface load (overthrust terrain, dark shade) is required to flex down the basement sufficiently to match the observed depth to the present-day base of the foreland basin sequence and explain the gravity low. Crustal thinning is required to fit the Bouguer anomaly gradient and part of the amplitude of the gravity high. The amount of crustal material removed as a result of thinning can be estimated from the difference between the model Moho and that predicted assuming that the flexure of the basement is reflected in the Moho config-

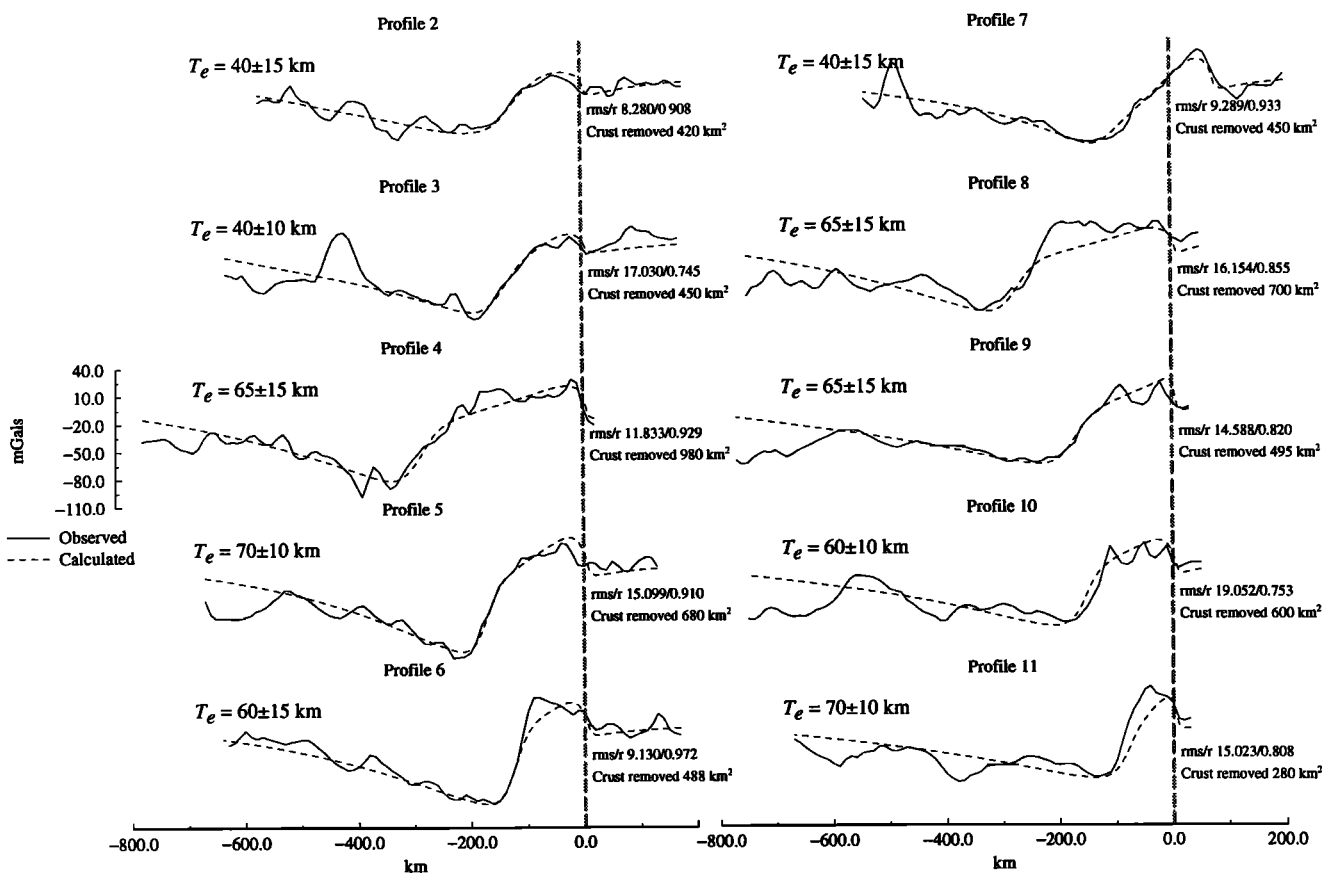


**Figure 4.** Summary of observed (solid) and calculated (dashed) Bouguer anomalies stacked on the position of the plate break (thick grey line) for 10 profiles from the southern Appalachians. The rms residual and $r$ correlation coefficient are shown. Also shown is the area of crustal material removed from the base of the crust.

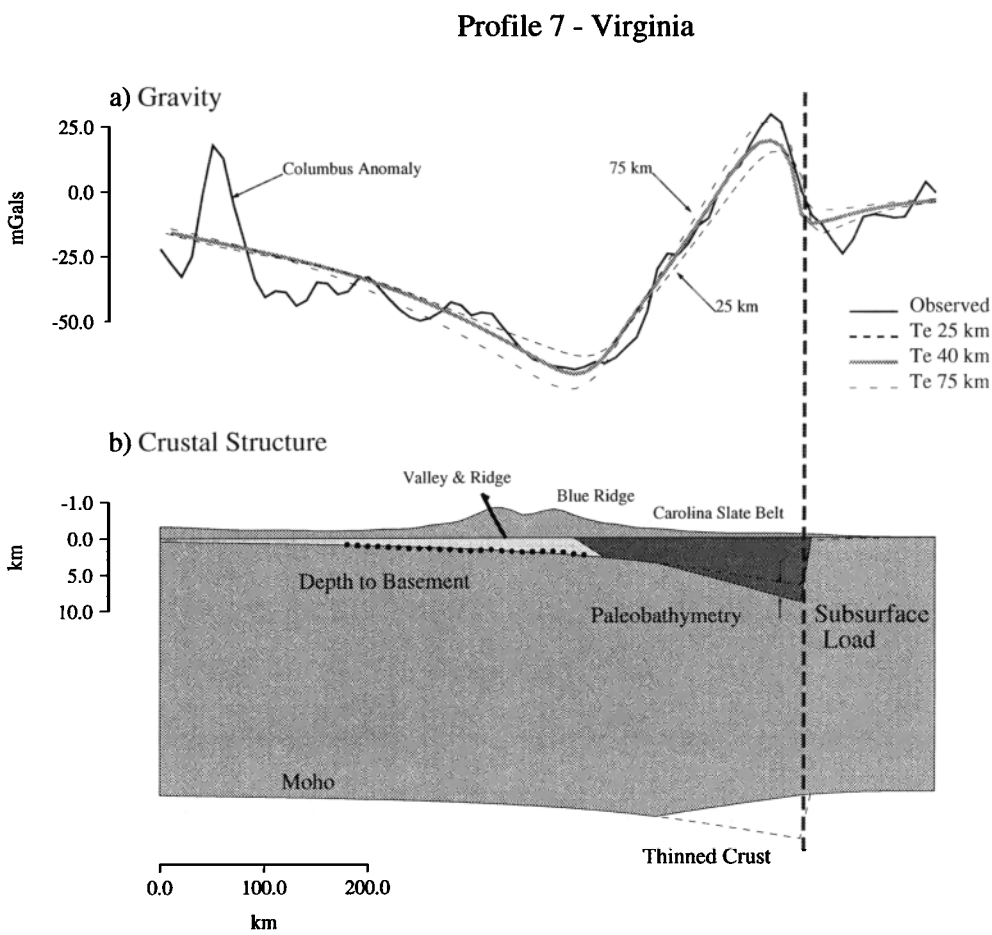


**Figure 5.** (a) Observed and calculated Bouguer gravity anomalies for a profile from the Virginian Appalachians. A best fit $T_e$ of 40±15 km is found. The origin of the Columbus Anomaly is discussed in the text. (b) Crustal structure for this $T_e$. There is good agreement between calculated and observed (dots) depth to basement. The crustal thinning implied (difference between lower dashed line and modeled Moho) suggests that the Carolina Slate Belt overthrusts the Paleozoic North American margin. Heavy grey dashed line shows the plate break. Dark shade, subsurface load 2850 kg $m^{-3}$; middle shade, crust 2670 kg $m^{-3}$; light shade, sediment infill 2500 kg $m^{-3}$.

uration (lower dashed line). Figure 5a shows the sensitivity of the gravity anomaly to variations in $T_e$ and indicates that a $T_e$ of 40 km is the best fit overall. A $T_e$ of 25 km could also explain the gravity data, but 75 km could not.

Figure 6 summarizes the results from Figure 4. A variation in $T_e$ of 40-70 km along the length of the mountain range is found. We cannot resolve variations in $T_e$ in the direction perpendicular to the strike of the mountain range. These results are in agreement with the lower end of the estimates of *Karner and Watts* [1983] and the upper end of the spectrally derived (coherence) estimates of *Bechtel et al.* [1990], who found a $T_e$ of ~ 35 to 50 km, but with no variation along the length of the mountain range.

## Andes

The locations of the profiles studied are shown in Figure 2. The $T_e$ structure and the applied vertical shear force are allowed to vary. The magnitude of the shear force is of order 1-3x$10^{12}$ N $m^{-1}$.

To illustrate the method by which we infer lateral variations in $T_e$, we consider a profile from Ecuador shown in Figure 7. The vertical heavy dashed line of Figure 7 shows the position of the plate break.

Figure 7a shows the topography from the two data sets (SAGP and DTM3). The topographic data sets agree well except at the shortest wavelengths. This is the load which is placed on broken plates of various constant thickness. Figure 7c shows the observed Bouguer anomalies and anomalies calculated for constant thickness plates of 5, 25, and 50 km. The large positive Bouguer anomaly at the western end of the profile is probably a result of obduction of Pacific oceanic crust. A $T_e$ of 5 km fits the data well beneath the mountainous region. A $T_e$ of 25 km fits better in the sub-Andean region and a $T_e$ of 50 km fits that part of the anomaly farther out in the foreland. From this we infer that

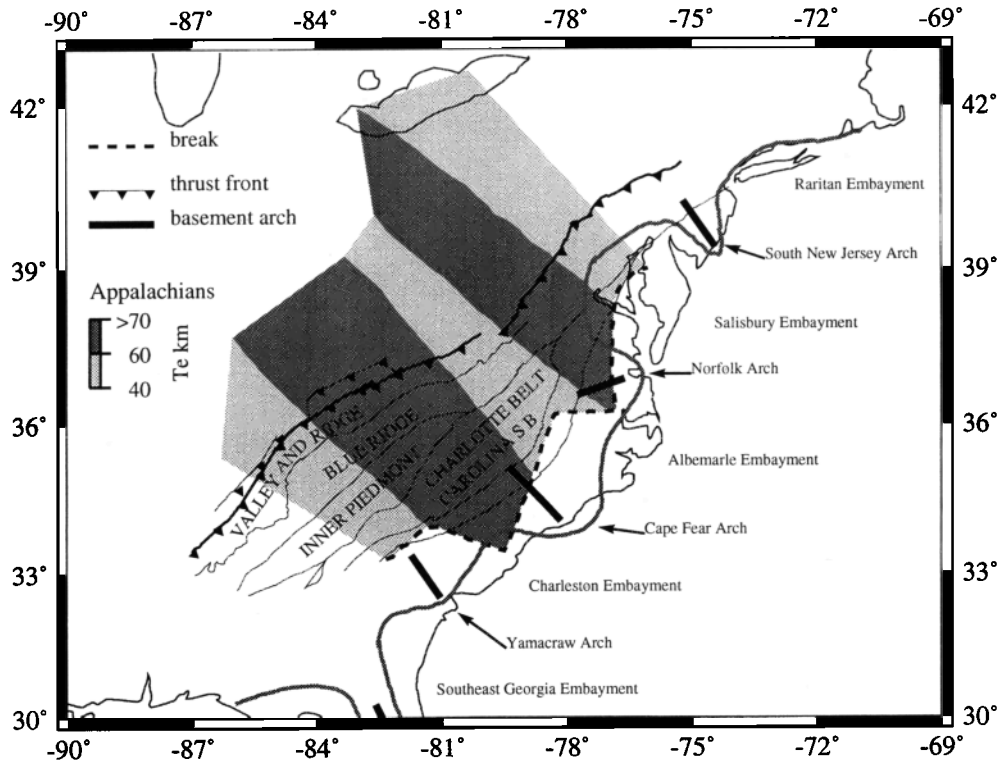


**Figure 6.** Contour map of $T_e$ in kilometers for the Appalachians. Heavy dashed line shows the position of the plate break. The heavy coastal grey line shows the architecture of the present-day passive margin which is a series of embayments and arches from *Ward and Strickland* [1985]. Other lines as in key. There is significant segmentation of strength along-strike of the mountain range.

the $T_e$ varies from low values beneath the mountain to high values in the foreland, as shown in Figure 7b. We compute the gravity anomaly using this $T_e$ structure and an end force of $0.5 \times 10^{12}$ N m$^{-1}$. An improved fit between observed and calculated anomalies is found as shown by the thicker line in Figure 7c and apparent in the decrease in the rms residual and increase in $r$.

This procedure is repeated along all the profiles across the mountain chain shown in Figure 2. The profiles in Figure 8 and 9 show the results for gravity together with the $T_e$ "tie points" (underlined) where we define changes in $T_e$. We linearly interpolate between these points and then apply a smoothing cosine filter to construct the $T_e$ profiles.

Published stratigraphic data for the sub-Andean foreland basins are limited. Commercial data were obtained (S. Lamb, personal communication, 1995) for the Beni foreland basin in Bolivia for the depth to the base of the Cretaceous in two way travel time. This was converted to true depth using velocity functions obtained from a regional exploration seismic line through the region. Profile 41 passes through the Beni basin, and the results of the analysis from this profile are shown in Figure 10. Figure 10a shows the topography from the two data sets. The best fitting $T_e$ structure shown in Figure 10c determined from gravity analysis as shown in Figure 10b is used to calculate the expected flexure of the basement shown in Figure 10d. Figure 10d shows that the position of the flexed basement (solid thick line) matches the observed depth to basement (circles) extremely well and no change in the $T_e$ structure is required. The Beni basin therefore appears to lie on a gradient of $T_e$. Figures 10b and 10d also show the expected deflection and gravity profiles for different $T_e$. Although a constant $T_e$ of 75 km could explain the observed gravity anomaly, it cannot match the observed depth to basement.

Figure 11 shows the results of Figures 8 and 9 as a contour map of $T_e$. The positions of the cratonic shield areas are approximately delimited in Figure 11 by the outlines of the sub-Andean foreland basins and the Amazon rift basins. The Central Brazilian Shield appears strong with a $T_e$ of up to 85 km. This high strength region appears to extend under the Beni and other foreland basins of the Bolivian Andes. High $T_e$ underlies the eastern edges of the Llanos and Barinas Apure basins. The northern Peru/Ecuador region is somewhat complicated with higher $T_e$. A weak zone in southern Peru is observed which coincides with the landward trend of the Nazca Ridge. A decrease away from the bend region is observed, with the lithosphere to the north appearing stronger than that to the south.

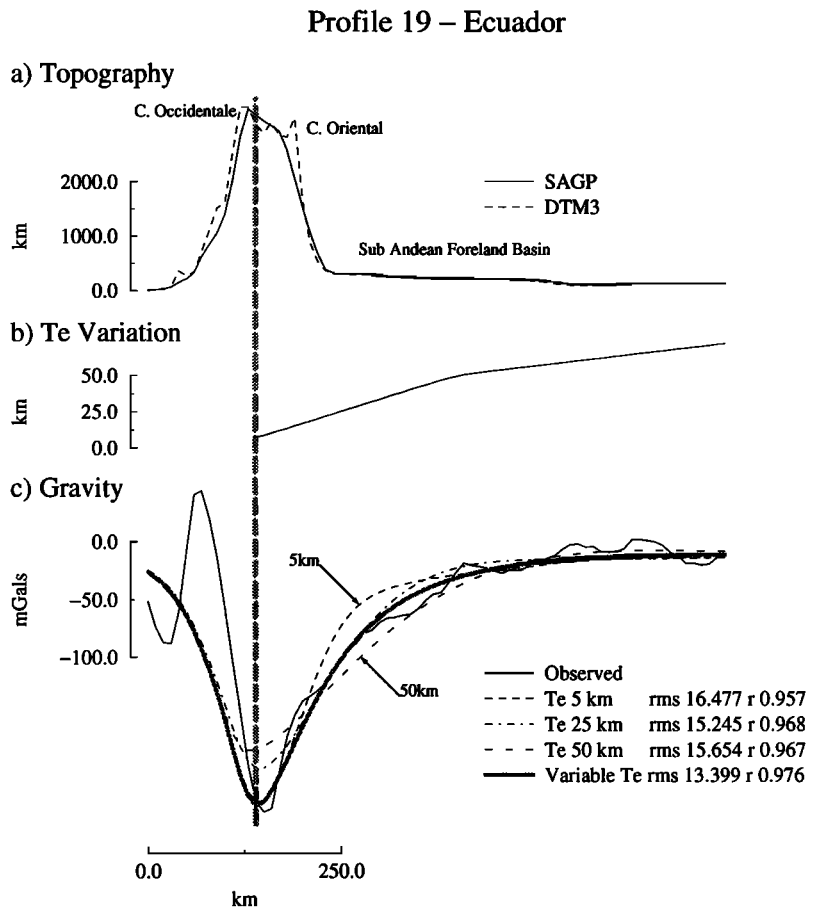


**Figure 7.** (a) Observed topography from South American Gravity Project data set and the GETECH 3 arc min Digital Terrain Model. (b) Best $T_e$ structure calculated from gravity analysis. (c) Observed (heavy solid) and calculated Bouguer anomalies (various dashed) for various constant $T_e$. The thicker line shows the gravity anomaly calculated using the best $T_e$ structure of Figure 7b and an applied end force of $0.5 \times 10^{12}$ N m$^{-1}$. The heavy dashed line in all figures shows the position of the break.

These conclusions are in agreement with the inferences of *Whitman* [1994] and *Watts et al.* [1995], although we conclude that the regions north and south of the bend have significant strength.

## Resolution of $T_e$ Variation

In order to quantify the magnitude and likely location of errors in the trial and error solution, we use an inverse method to find the best $T_e$ structure and applied end shear force from the observed Bouguer anomaly. The plate break is as defined previously. The gravity anomaly is calculated from the flexure that results from the topographic load and any required end force on a variable thickness elastic plate. $T_e$ variation and applied end force are varied until a minimum misfit between observed and calculated gravity anomaly is reached (see the appendix for details of the minimization technique).

Figure 12 shows the results of inversion of a number of Bouguer anomaly profiles for $T_e$ and applied end shear force. For profile 47 from the southern Bolivian Andes the inverse solutions agree with the solution obtained by trial and error beneath the mountain and are independent of the initial parameter estimates (see Figure 12b). It is only when the observed Bouguer anomaly begins to flatten off toward the foreland that significant discrepancies arise between inverse and trial and error solutions. Unfortunately, the effect on the calculated gravity anomalies of this discrepancy in Figure 12c is small as seen by the minor changes in rms residual and $r$. In this region a wide range of $T_e$ estimates could therefore fit the observed anomalies equally well. However, we are able to exercise a geologically reasonable upper limit on the recovered $T_e$. The general increase in $T_e$ away from mountain range inferred in the previous section is recovered by the inverse method for a number of profiles shown in Figures 12d-12f. For example, Figure 12d shows the $T_e$ variation for profile 19 which was discussed in the previous section. The variation from the inverse method agrees with that from trial and error in the region where $T_e$ is recoverable, and the magnitude of the applied end forces are similar.

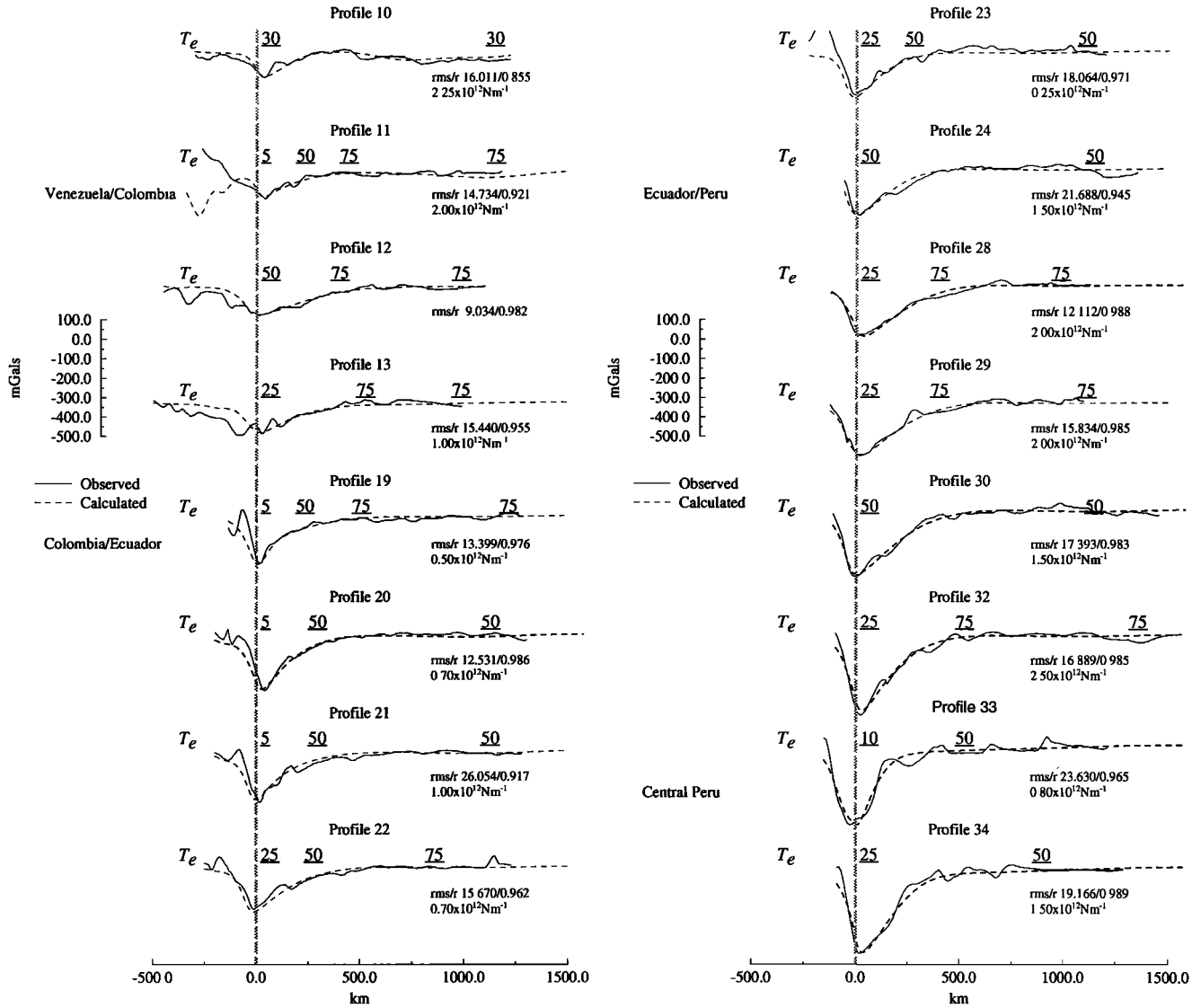


**Figure 8.** Summary of observed (solid) and calculated (dashed) Bouguer anomalies for 16 profiles from the northern Andes. Underlined numbers are $T_e$ "tie points" which are used to construct the $T_e$ profile. Profiles are stacked on the position of the plate break, shown by the heavy dashed grey line.

## Alpine-Carpathian Arc

The locations of the profiles studied are shown in Figure 1b. The results and possible range of $T_e$ and amount of any crustal thinning required are shown on Figure 13. It is not found necessary to vary the $T_e$ along each profile as observed Bouguer anomalies can be modeled with a constant value of $T_e$. However, as we move from one profile to another, different values of $T_e$ are required.

We attempted a similar analysis along the entire length of the Carpathian arc but we were only partly successful. Profiles through the Czech/Slovak Carpathians are complicated by the Bouguer gravity anomaly low associated with the Polish trough to the north. Profiles extending onto the Ukrainian foreland are complicated by positive Bouguer anomaly swells that trend in the same direction as the Trans-European and Caledonian faults (from the Black Sea to the Baltic Sea). These major fault zones separate the Precambrian East European Platform from the Phanerozoic central Europe platform. Magsat data [*Taylor and Ravat*, 1995] reveal a similarly orientated long-wavelength magnetic anomaly.

However, good stratigraphic data are available for the depth to the base of the Eastern Carpathian foredeep (isopach map of *Royden and Horváth* [1988]). These data are used to estimate $T_e$, and we find like *Royden and Karner* [1984] that the topographic load is insufficient to produce deflections that match the stratigraphic data. Therefore an additional shear force is applied at the end of the broken plate and of magni-

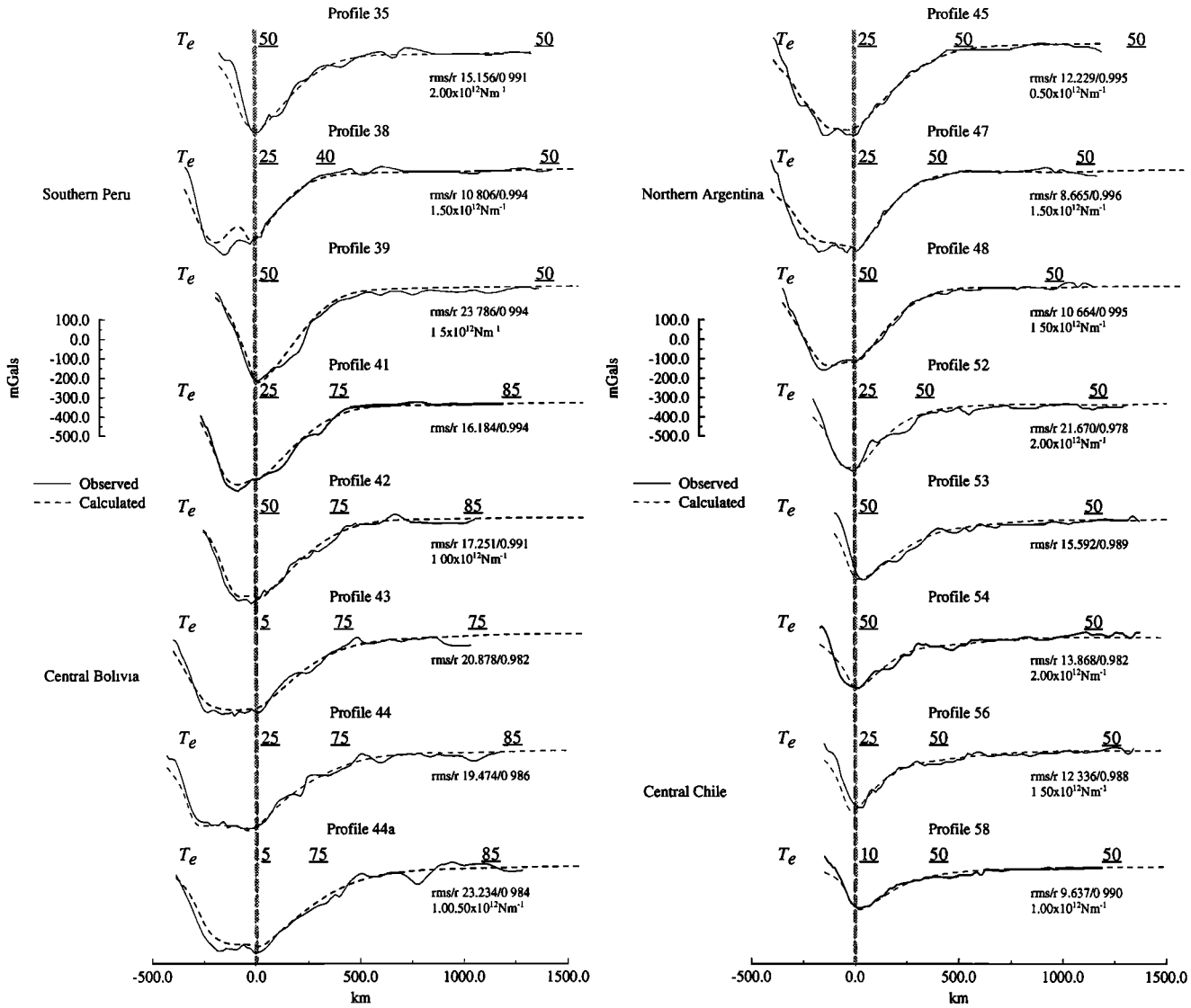


**Figure 9.** Summary of observed (solid) and calculated (dashed) Bouguer anomalies for 16 profiles from the southern Andes. Underlined numbers are $T_e$ "tie points" which are used to construct the $T_e$ profile. Profiles are stacked on the position of the plate break, shown by the heavy dashed grey line.

tude 0.5-1.5x$10^{12}$ N $m^{-1}$. *Royden and Karner* [1984] link this additional force to the the negative buoyancy of the subducted slab or dynamic effects. The density of the infill varies in the vicinity of the foreland basin from 2500-2600 kg $m^{-3}$. The results for deflection and gravity are shown in Figure 14. The fit for gravity is reasonable on some of the profiles whereas the fit for deflection is good for all profiles.

The results for the Alps and the Carpathians are shown contoured in Figure 15. We cannot resolve variation in $T_e$ in the direction parallel to the profiles. In the western Alps (approximately west of 9°W), $T_e$ is in the range 5-25 km with the lowest values occurring in a band extending out of central Switzerland. Another low strength area is seen in SE France in the vicinity of the southern Massif Central. How this area relates to the stronger region in central France is uncertain, as $T_e$ estimates from profiles 3 to 5 proved inconclusive. From Switzerland through the eastern Alps, $T_e$ increases from $\sim$ 10-15 km to $\sim$ 25-30 km.

Our results are lower than those of *Karner and Watts* [1983] and *Gutscher* [1995] in the eastern Alps and similar in the western Alps. The low values in Switzerland are consistent with the estimate of *Sinclair et al.* [1991] of the flexural strength of the foreland at 17 Ma. The results are lower than those of *Macario et al.* [1995] for the western Alps (their estimate of $T_e \sim 31$ km) and slightly lower for the eastern Alps ($T_e \sim 35$ km). However, we disagree with them and conclude that there is evidence for an increase in $T_e$ from the central Alps of Switzerland and western Germany toward eastern Germany. Based on deflection data alone, *Gutscher* [1995]

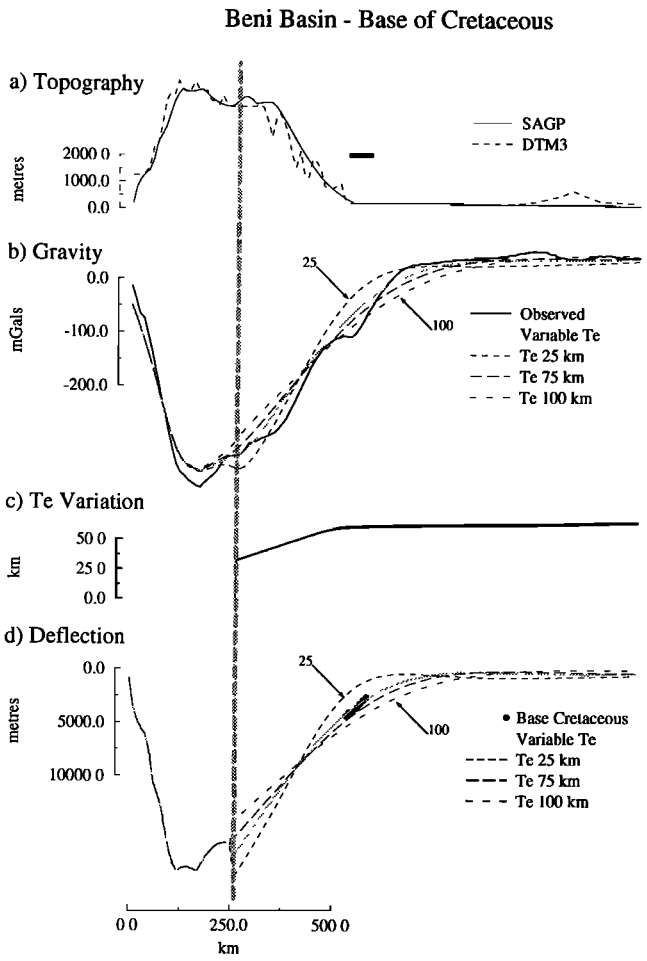


**Figure 10.** (a) Observed topography from SAGP data set and DTM. Heavy horizontal line shows the position of the Beni basin, one of the sub-Andean foreland basins. (b) Observed Bouguer anomaly (solid) and calculated gravity anomalies for different $T_e$ (variously dashed). (c) Best $T_e$ structure determined from gravity analysis. (d) Observed (circles) and calculated depths to the base of the foredeep sequence (base of Cretaceous). Heavy dashed grey line in all figures shows the position of plate break.

also concludes that there is evidence for an increase in $T_e$ toward the eastern Alps.

In the Romanian Carpathians, we can compare our results with the work of *Royden and Karner* [1984] whose one profile through the center of the Romanian Carpathians was modeled with a constant $T_e$ of 30 km and an additional shear force of $1.5 \times 10^{12}$ N m$^{-1}$. Their model, however, predicts very large flexural forebulges, suggesting that too rigid a plate has been bent to high curvatures to explain the observed data. In addition, they do not model the gravity. We prefer a model where $T_e$ varies and the forebulge from the weaker part of the plate is damped by the stronger part of the plate. *Cloetingh and Burov* [1996] cite $T_e$ estimates in the Carpathians in the range 5-45 km. Our modeling tends to confirm the lower end of these previous estimates.

## Two-Dimensional Modeling

In the previous section we inferred spatial variations in $T_e$ from forward modeling of gravity anomaly and stratigraphic profiles. In this section we first show that constructing such maps from 1-D profiles is valid. Then we use a simple stratigraphic model to show how spatial variation of $T_e$ exerts a strong influence on foreland basin geometry and stratigraphy. The partial differential equation for bending of a thin elastic plate of variable thickness is solved using a finite difference scheme outlined in the appendix.

### Recovery of 2-D Variation From Profile Analysis

Figure 16 is a hypothetical map of $T_e$. We first apply a uniform cross-section load (Gaussian of height 1000 m, halfwidth 100 km, centered on $x$=200, shown on Figure 17a) and calculate the expected gravity anomalies over the entire region. Then, a profile perpendicular to the load is selected (profile CC′ in Figure 16). Using the inverse method outlined above, the 1-D $T_e$ variation along the profile is recovered and it compares well with the actual variation (Figure 17b). A negligible shear force is required. These results suggest that it is possible to recover the 2-D variation of $T_e$ using the profile method. There is effectively no difference between observed and calculated gravity anomalies (Figure 17c). The largest discrepancies between actual and recovered $T_e$ occur at the western end of the profile where the gradient of the gravity anomaly is too low to recover $T_e$. Figure 17d shows that when the infill density is unknown the real variation is obviously not recovered. However, the general increase in $T_e$ away from the load is still recovered. We note that the load must, however, be of reasonably uniform cross section and profiles need to be extracted perpendicular to the local strike of the load.

### Stratigraphic Model

The map of $T_e$ in Figure 16 represents a $T_e$ structure similar to that observed in many continents. There is a core of high $T_e$, corresponding to a craton, surrounded by lower $T_e$.

A simple stratigraphy is modeled by allowing a topographic load with a frontal slope of ~1.5° to migrate across the western part of this region in ten 30 km steps. As the topographic load is emplaced, a foreland basin and flexural bulge are created. Between steps, it is assumed that the basin is filled to sea level with sediments and that flexural bulges are eroded. The exact processes of erosion and sediment transport are not modeled. The synthetic stratigraphy developed for each of the sections is shown in Figure 18. In reality, thrust migration would incorporate and destroy the earlier stratigraphy development, and only the later stages of foreland basin development would be preserved undeformed.

The shape of the foreland basins (light shade in Figure 18) and the overall geometry of the basement de-

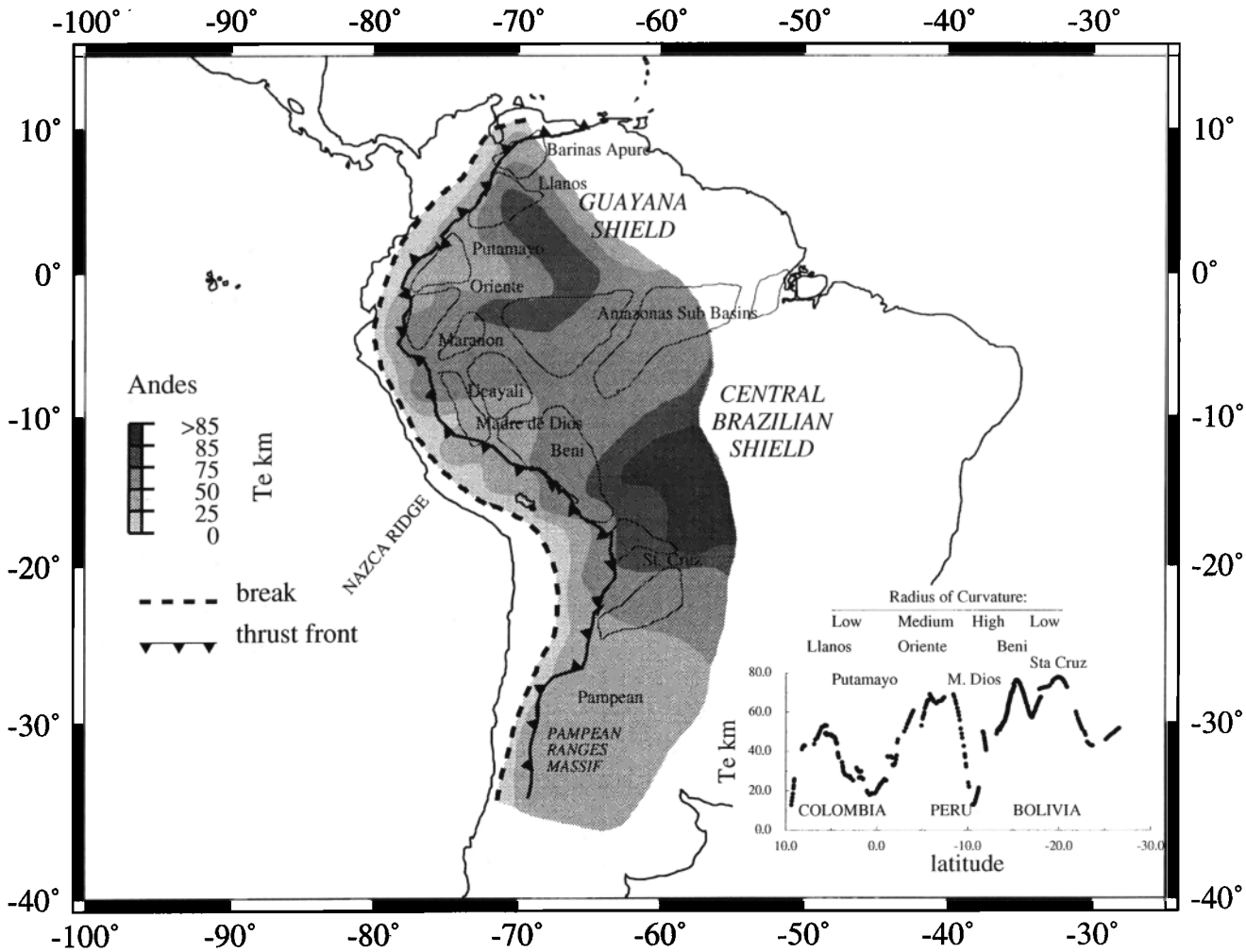


**Figure 11.** Contour map of $T_e$ in kilometers for the Andes. The thick dashed line shows the position of the break. Other lines as in the key. The outlines of the sub-Andean foreland basins and Amazon rift basins are from *Chigne and Hernandez* [1990]. Inset shows $T_e$ at the thrust front as a function of latitude. Also qualitatively shown is the local radius of curvature of the thrust front and location of the main sub-Andean basins.

flection developed are quite different. For both profiles the shape of the foreland basins developed increases through time as the topographic load builds up with earlier basins much smaller than later basins, developing on more rigid lithosphere. The size of the basins developing on the southern part of the region (profile BB′) are much smaller than those to the north (profile AA′). There is a large variation in width of the basin from north to south. Facies would correspondingly migrate by a similarly large amount, and we would expect to see pronounced along strike variations in stratigraphy. Figure 18b shows a much steeper basement deflection than Figure 18a and overall more localized deflection. The regional dip of strata in each case would be quite different and this may offer some control on fluid migration.

## Discussion

### $T_e$ and Thrust/Fold Belt Curvature

*McNutt et al.* [1988] compiled all previous reliable estimates of $T_e$ at continental thrust belts (from forward modeling of gravity anomaly and deflection data). This compilation appeared to show a linear relationship between elastic thickness and logarithm of the radius of curvature of the thrust front. They claim that the curvature of the thrust front in plan view is echoed in the bending of the underthrust plate in the plane of the Earth's surface. However, it is not obvious why the geometry of the underthrust plate should be related to the curvature of the thrust front. The position of the thrust front simply shows how far over the foreland lithosphere deformation has proceeded. Thin skinned deformation

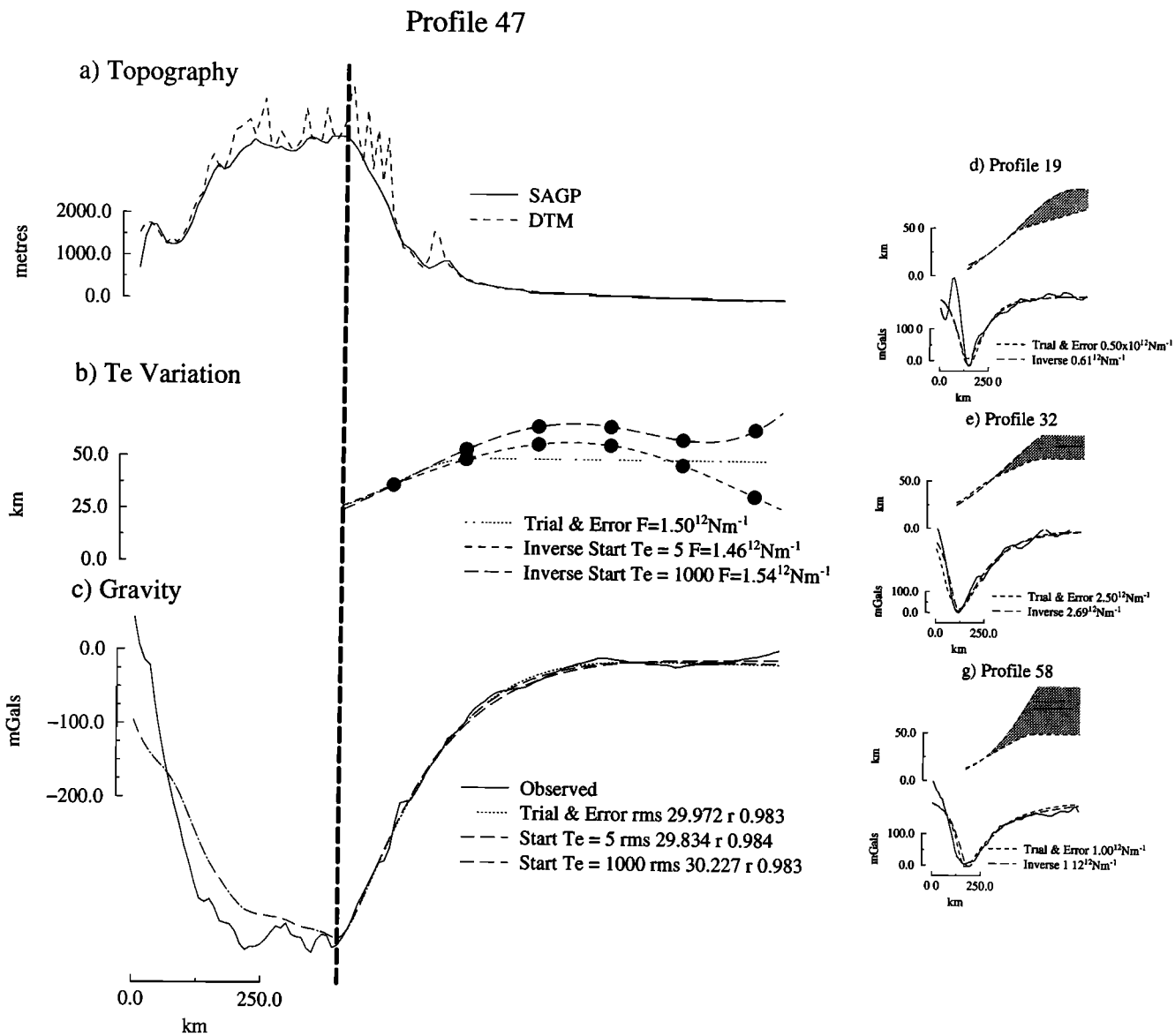


**Figure 12.** Inverse method applied to profile 47 in the southern Bolivian Andes. (a) Profiles of topography from the two data sets. (b) Trial and error and inverse solutions for $T_e$. Solid circles on the inverse solution show the location of the Gaussians used to construct the $T_e$ function. Inverse solution is independent of starting position in the region where $T_e$ can be recovered. Also noted are the end forces required for each solution. (c) Observed and calculated gravity anomalies for the $T_e$ variations shown in Figure 12b. (d)-(f) Profiles of $T_e$ variation (top) and gravity anomalies (bottom) for three further profiles, together with the end forces required. The grey shades indicate the range of possible $T_e$ values.

could produce rapid thrust advance in one area, causing the thrust front to bulge out locally and decrease its radius of curvature. Because thin skinned deformation is relatively shallow, there is no requirement for the underthrust lithosphere to be bent into a tighter curvature to accommodate large amounts of shortening.

As the inset in Figure 11 shows there is little relationship between $T_e$ at the thrust front and local curvature in disagreement with the conclusion of *McNutt et al.* [1988]. For example, in the Bolivian Andes the radius of curvature of the thrust front is low and $T_e$ is high. Also, our studies show that $T_e$ varies perpendicular to the thrust front, indicating that it is difficult to assign a single value of $T_e$ to the local radius of thrust front curvature.

### Stratigraphy and Sea Level Curves

Some parts of the sea level curve [*Vail et al.*, 1977; *Haq et al.*, 1987] are constructed from foreland basins which have become connected to the global ocean system. The vertical distance between onlapping chronostratigraphic horizons is interpreted in terms of a change

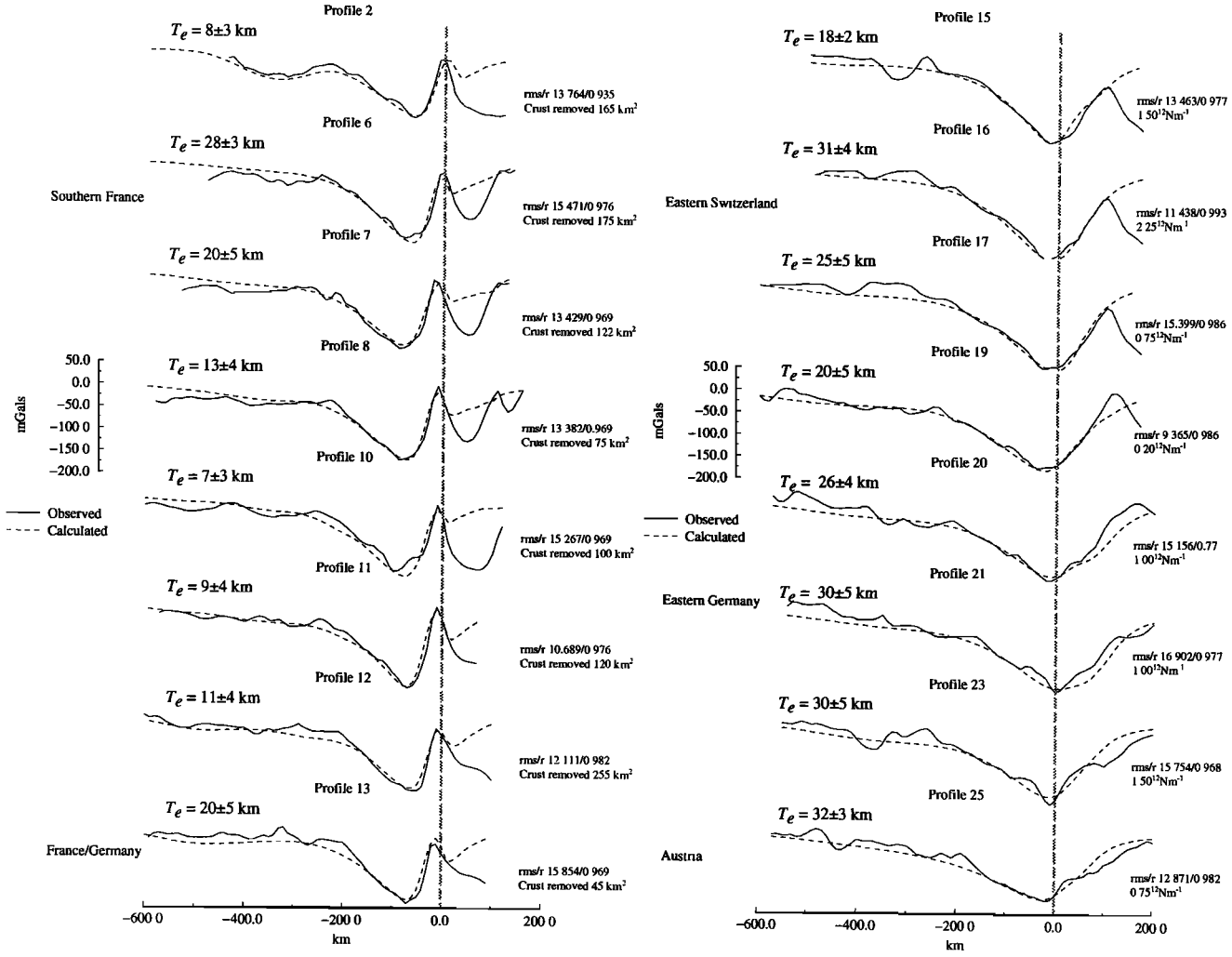


**Figure 13.** Summary of observed (solid) and calculated (dashed) Bouguer anomalies stacked on the plate break (heavy dashed grey line) for 16 profiles from the Alps.

in relative sea level. Figure 18 shows that large differences in the pattern of onlap occur along strike of a foreland basin simply because of spatial variations in the strength of the underlying lithosphere. Therefore it would be difficult to use sea level curves from individual localities to construct a global relative sea level curve as was done by *Haq et al.* [1987] for the Cretaceous sea level from the Western Interior Seaway of the Rockies foreland. We believe that some of the inferred relative sea level changes in the Cretaceous, which are difficult to explain by glacial eustasy, may be the result of a local flexural control.

## $T_e$, Geothermal Gradient, and Heat Flow

According to the multilayered rheological models of *Burov and Diament* [1995], the base of the mechanical continental lithosphere approximately follows the 700°C isotherm. At temperatures greater than this, thermally activated power law creep processes rapidly dissipate deviatoric stresses so that the lithosphere has zero strength. They show that elastic thickness is an equivalent measure of the integrated strength of this strong part of the lithosphere. They realize that it is unlikely that thermal effects can result in a reduction of $T_e$ to very low values as an extremely high geothermal gradient would be required to bring the 700°C isotherm to within approximately 10 km of the surface. To explain these very low values of elastic thickness, they conclude, along with other workers [e.g., *Kusznir et al.*, 1991; *Watts*, 1992], that $T_e$ must reside in the mechanical crust whose thickness is given by the depth to a lower isotherm such as the 200-300°C isotherm. Some form of decoupling must operate to remove the contribution to lithospheric strength from the mantle.

Geothermal gradients would be expected to increase toward active tectonic regions such as mountain ranges. Because of the thermal control on $T_e$ outlined above, together with the possibility that heat flow might correlate inversely with $T_e$ [*Zoetemeijer et al.*, 1990; *Lowry and Smith*, 1994; *Hartley et al.*, 1996], part of the de-

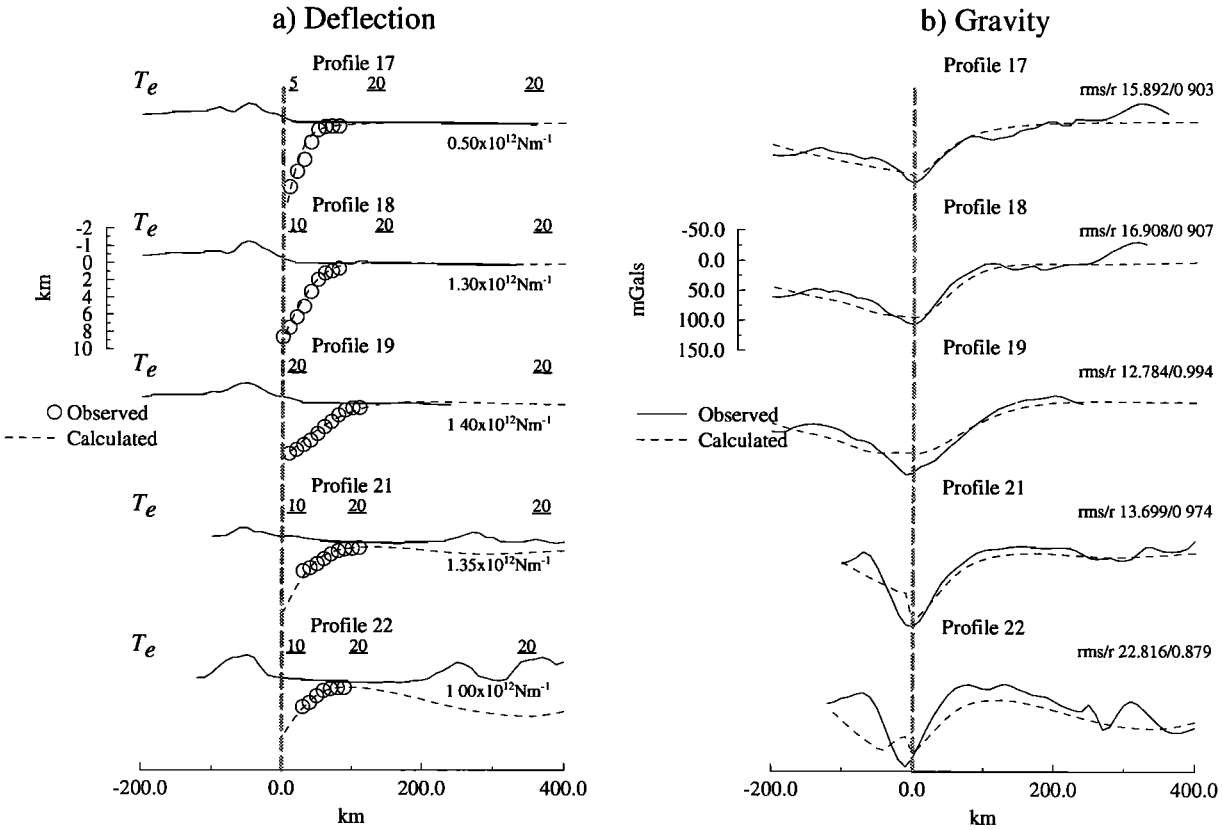


**Figure 14.** Summary of (a) observed (open circles) and calculated (solid) depth to base of foredeep with topography and (b) observed (solid) and calculated (dashed) Bouguer anomalies stacked on the position of the plate break (heavy dashed grey line) for five profiles from the Romanian Carpathians. Underlined in Figure 14a are $T_e$ "tie-points" which are used to construct the $T_e$ profile.

crease in $T_e$ toward the mountain range that we have found in the Andes and Carpathians could be explained in terms of increased geothermal gradients.

That there might a relationship between continental $T_e$ and heat flow is supported by our observations in the Alps. The Swiss Molasse basin (western Alps) has generally higher present day heat flow than the German Molasse Basin (eastern Alps) (see references of *Schegg et al.* [1997]). Also, *Schegg et al.* [1997], using vitrinite reflectance, have shown that Tertiary heat flow in the western Alps is higher than estimates for the eastern Alps. A decrease in heat flow from the west to east Alps correlates with our results in Figure 15 of an increase in $T_e$.

### $T_e$ and Inelastic Processes

Yielding of a constant thickness plate due to extreme bending under large loads will result in lateral variations in $T_e$. Significant yielding would be likely to occur in the foreland lithosphere of the Andes because the flexure profiles in Figure 10 show that curvatures are high, up to $1\text{x}10^{-8}$ m$^{-1}$. Curvatures of a similar magnitude have been proposed to lead to inelastic yielding at seamounts (up to $10^{-7}$ m$^{-1}$ beneath the load) [*Wessel*, 1993], ocean trenches ($\sim 2\text{x}10^{-7}$ m$^{-1}$ at the outer rise) [*Judge and McNutt*, 1991] and continental convergent zones [*Waschbusch and Royden*, 1992]. Undoubtedly, such reductions in observed strength contribute to the regional pattern of variation of $T_e$, at least in the case of the Andes and Carpathians. We cannot resolve whether curvature related yielding is important at the Appalachians and Alps since we can model the gravity data at these mountains with a uniform $T_e$ along individual profiles.

### $T_e$ and Tectonic Style

*Watts et al.* [1995] propose that the tectonic style of the orogen is influenced by the strength of the underlying lithosphere. As the orogen advances onto stronger lithosphere, more thin-skinned type fold and thrust deformation develops. This occurs because higher $T_e$ results in broader, shallower deflections of the foreland lithosphere which promote the development of low-angle décollement surfaces. In addition, being inherently stronger, the underthrust lithosphere will tend to resist being incorporated in deformation. Orogenic loading of weaker lithosphere will result in much steeper and narrower deflections, which intuitively would seem

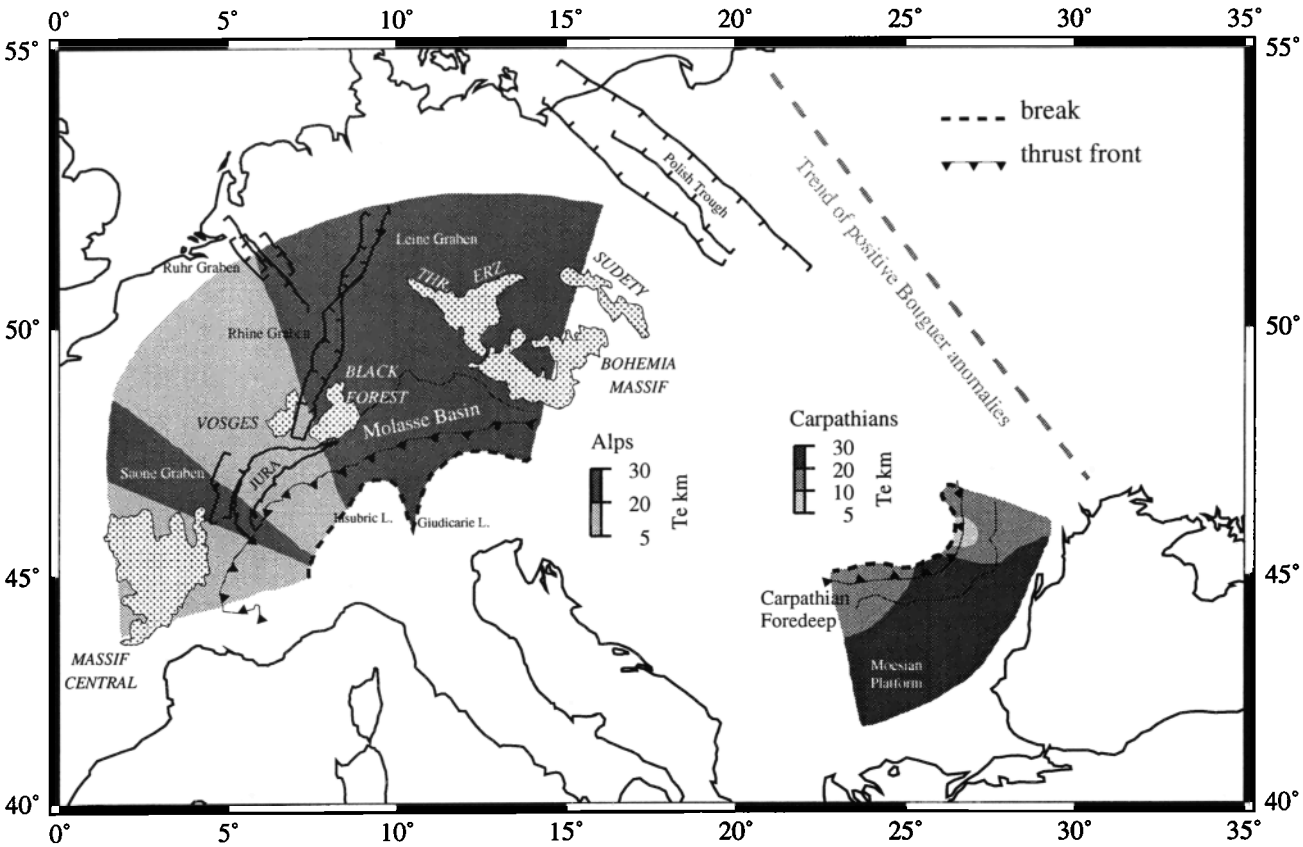


**Figure 15.** Contour map of $T_e$ in kilometers for the Alps and Romanian Carpathians. Solid line shows the position of the break in the plate. Other lines as in the key. In the Alps, the plate break corresponds approximately to the Insubric Line and its along strike continuation. THR Thuringer Wald, ERZ Erzgebirge.

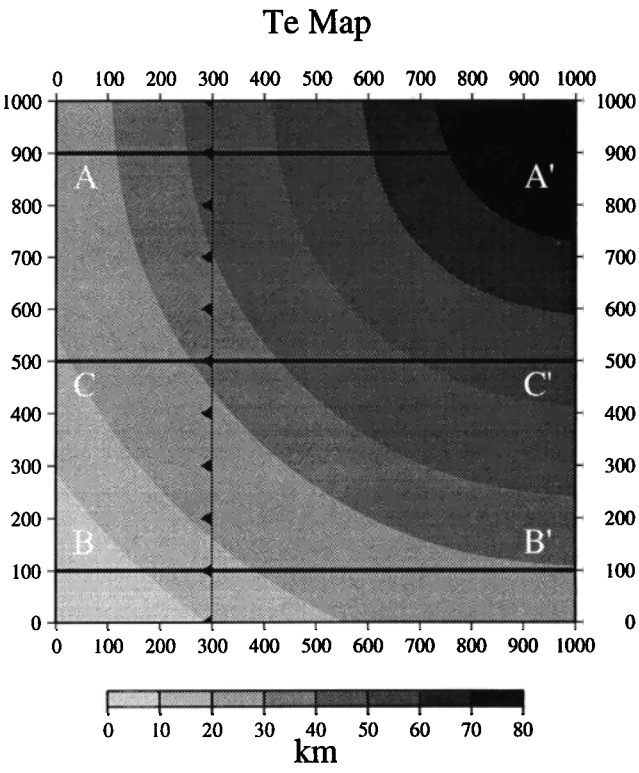


more difficult for thrust fronts to advance over. The lack of strength would also encourage the underthrust lithosphere to become involved in more basement type deformation. This relationship between $T_e$ and tectonic style is supported by our results in southern Peru and central Bolivia (Figure 11).

In the Alps there are significant structural changes from the west to east Molasse basin. In the Swiss part of the Molasse basin, shortening is thought to be more basement involved than to the east. This more basement involved deformation occurs above weaker lithosphere ($5<T_e<20$ km). Also, recent seismic evidence [*Pfiffer and Erard*, 1996] suggests that beneath the thin-skinned fold deformation of the Jura, deformation involves the basement. This suggests that although the

**Figure 16.** A hypothetical $T_e$ structure corresponding to a cratonic region. Profile CC′ is used to demonstrate the recovery of 2-D spatial variation of $T_e$ from profile analysis. Along profile AA′ and profile BB′ the results of the stratigraphic model are presented. The barbed line at $x = 300$ shows the final position of the thrust front in the stratigraphic model.

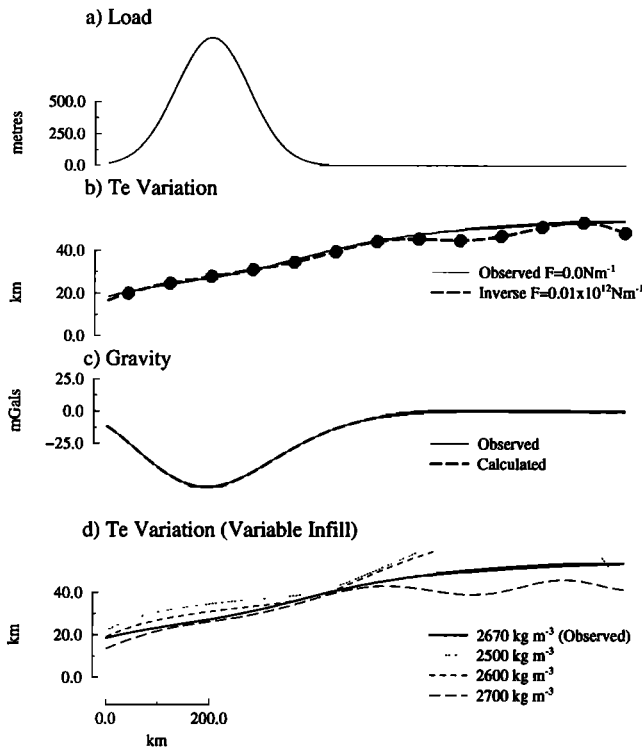


**Figure 17.** (a) Profile of load. (b) Observed and recovered $T_e$ along profile CC′ of Figure 16. Solid circles show the location of the centers of the Gaussians used to construct the $T_e$ function. Maximum discrepancy occurs where the gradient of the observed gravity anomaly is low. (c) Observed and recovered gravity anomalies along profile CC′. This shows that it is possible to recover most of the true $T_e$ variation using the profile method. (d) Observed and recovered $T_e$ profiles assuming different infill densities. The general sense of an increase in $T_e$ is recovered.

presence of a favorable horizon (shale, salt) may encourage décollement development, the basement strength and geometry (flexurally controlled) also appear to be an important control on tectonic style.

## Inheritance

An underlying theme of our discussion has been that because of the cyclic nature of plate tectonic processes (e.g., the Wilson cycle) the thermal and mechanical characteristics of the lithosphere persisting from a past event may exert a strong control on the development of a later event. The properties of the previous plate tectonic event may be inherited by the next event. For example, the strength variations that have been reported at passive margins may influence the geometry of the foreland basins and tectonic style occurring during continental collision.

Figure 19 shows that $T_e$ at rifts and passive margins are in the range 0-50 km, with a majority <25 km. Therefore relatively low $T_e$, compared to that of the adjacent craton, is a characteristic of stretched continental lithosphere. This is not surprising in view of the fact that rifting results in a thinning of the mechanical lithosphere. Because of irreversible plastic and ductile strain during rifting, the long-term strength of stretched lithosphere may be low.

We appeal to a transition from weakened rifted lithosphere to stronger cratonic lithosphere to explain the pattern of $T_e$ variation revealed from gravity modeling in the Andes. The actual passive margin itself may be included within this regional gradient of $T_e$ but at present, due to a lack of a detailed crustal structure and masking effects of variations in geothermal gradients and inelastic yielding, it is not possible to unequivocally state that the entire change in $T_e$ is due to this transition. However, the western side of South America has had a long history as a passive margin prior to the initiation of subduction [*Pitcher et al.*, 1985], so it is probable that some of the variation is a result of this transition.

In the Alps there is evidence that the precollisional $T_e$ structure of the Tethyan margin is recorded not only in the gravity anomalies but also in the stratigraphy of the Alpine foreland. For example, the thickness of Mesozoic sediments increases from east to west below the Molasse basin [*Bachmann et al.*, 1987]. This suggests that lithospheric thinning increases in the same direction which may therefore offer another explanation for the decrease in $T_e$ from east to west that was required by the gravity modeling. In addition, there are a greater number of Permo-Carboniferous troughs in the western part of the Molasse basin than in the east [*Brink et al.*, 1992].

In the Appalachians we have also observed segmentation of strength. The relatively low $T_e$ segments are coincident with NW-SE trending Bouguer anomaly highs (e.g., the Columbus anomaly on Figure 5a). These are thought to be related to rift structures in the Grenvillian basement (H. C. Noltimier, personal communication, 1996). We suggest that these strength variations exerted a control on Paleozoic passive margin formation which caused a strongly segmented transform dominated style to develop [*Thomas*, 1991]. We speculate that these strength variations may even have played some role in the development of the present-day North American margin structure of embayments and arches (heavy coastal line in Figure 6) which controlled the Mesozoic and Cainozoic stratigraphic developed of the margin.

Our modeling of the Appalachian gravity "high" requires crustal thinning. Therefore mapping of the "high" provides an estimate of the location of the position of the Paleozoic passive margin of the North American continent as suggested by *Cook and Oliver* [1981]. An outstanding problem, therefore, is why the Appalachians, which developed on extended lithosphere, have a high $T_e$ (in the range 40-70 km ) rather than low values such as observed at rifts and passive margins. There is evidence that $T_e$ of the Appalachian foreland

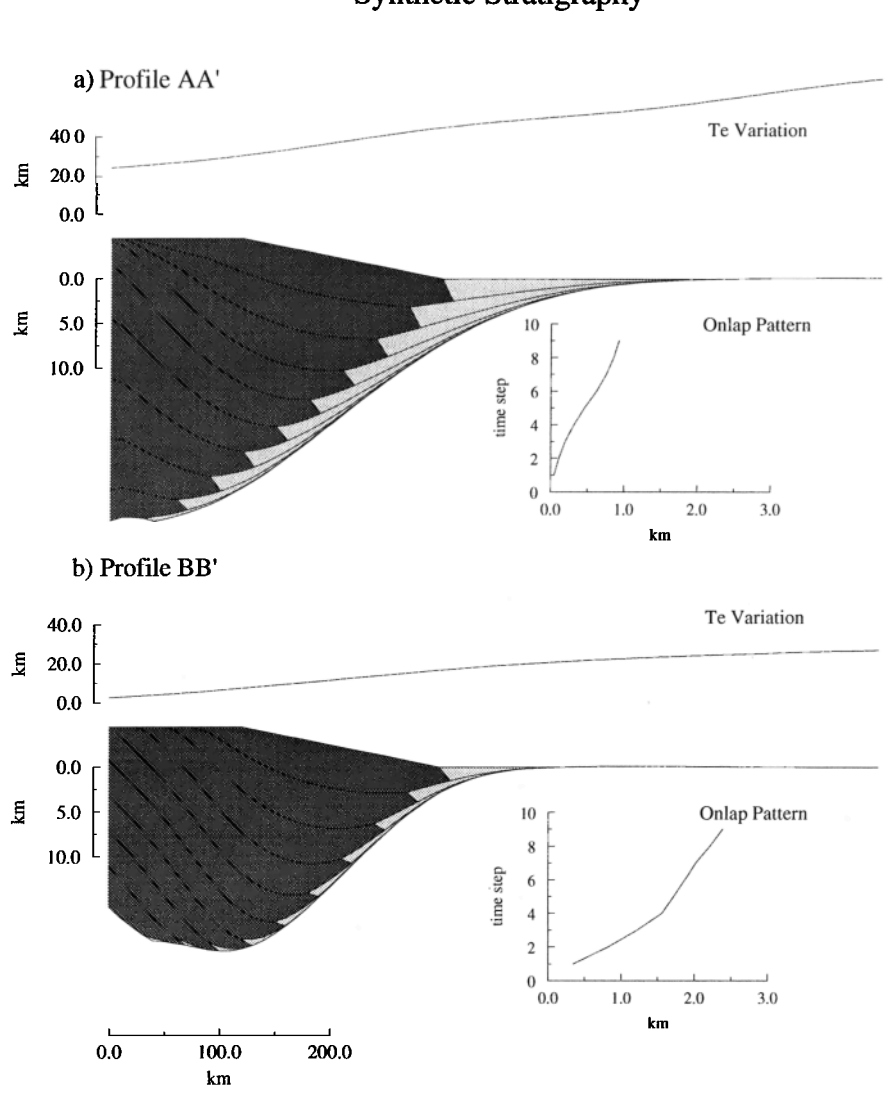


**Figure 18.** Synthetic stratigraphy developed as a topographic load advances across the hypothetical $T_e$ structure shown in Figure 16. (a) Stratigraphy developed along AA'. (b) Stratigraphy developed along BB'. In each, the top panel shows the $T_e$ profile the load advances across. The bottom panel shows the stratigraphy developed where the light shades represent rocks of the foreland basin and the dark shades represent rocks of the fold and thrust belt. Insets on both show onlap curves which can be interpreted in terms of sea level variations.

lithosphere was low during the Paleozoic. For example, recent interpretations of Appalachian stratigraphy [*Bradley and Kidd*, 1991; *Diecchio*, 1993] suggest that the width of this foreland basin was much narrower and the location of the peripheral bulge much closer to the thrust front than proposed by earlier models [e.g., *Quinlan and Beaumont*, 1984].

It is also interesting to note that no low values of $T_e$ have been estimated from any other Paleozoic orogen using methods which are based on the present-day curvature of the lithosphere. These methods include gravity modeling and comparison of calculated basin shapes to observed basin geometries. Using such methods for the Paleozoic Urals, *Kruse and McNutt* [1988] calculate a $T_e$ of $\sim$ 50-100 km. However, low values of $T_e$ have been observed at active or recently active orogens today using both of these methods (e.g., Alps, Andes, Apennines [*Royden and Karner*, 1984]). This suggests that either (1) all ancient weak orogens are preferentially destroyed and removed from the geological record, or (2) stretched lithosphere that was weak at the time of orogeny is able to recover its strength. We speculate that this strength recovery requires that a long time has elapsed since rifting (Figure 19).

## Conclusions

We can draw the following conclusions from these studies of continent-wide gravity anomaly and topography data sets.

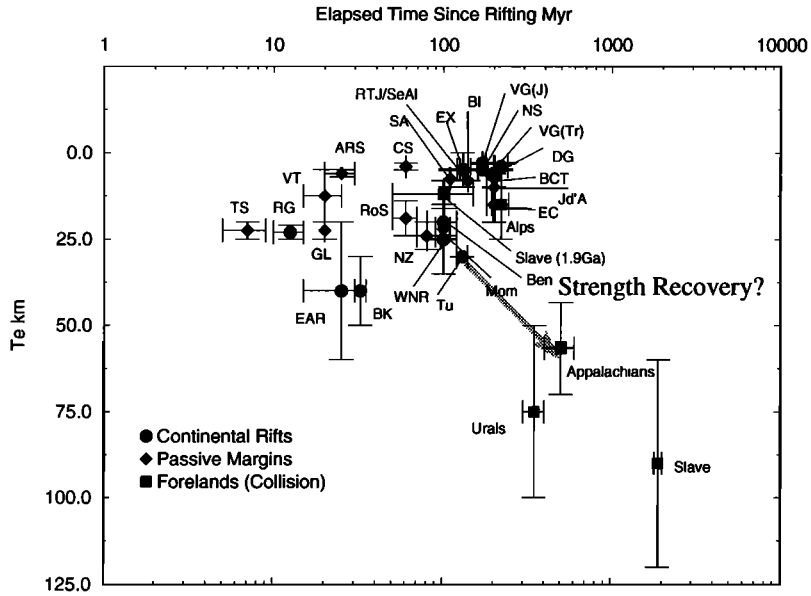


**Figure 19.** Graph of elapsed time since rifting in millions of years versus $T_e$ for three stages in the Wilson Cycle (circles, continental rifts; diamonds, passive margins; squares, foreland lithosphere involved in continental collision). BCT, Baltimore Canyon Trough [*Watts*, 1988]; EC, East Coast, United States; CS, Coral Sea; SA, South Africa [*Karner and Watts*, 1982]; EX, Exmouth Plateau [*Fowler and McKenzie*, 1989]; VT, Valencia Trough [*Watts and Torné*, 1992; *Janssen et al.*, 1993]; Jd'A, Jeanne d'Arc; VG(Tr) and VG(J), Viking Graben (Triassic, Jurassic) [*Kusznir et al.*, 1991]; NS, North Sea Central Graben [*Barton and Wood*, 1984]; BI, Bay of Biscay [*Diament et al.*, 1986]; TS, Tyrrhenian Sea [*Spadini et al.*, 1995]; NZ, New Zealand Western Platform [*Holt and Stern*, 1991]; GL, Gulf of Lions [*Kooi et al.*, 1992]; RTJ, Recôncavo-Tucano-Jatobá [*Magnavita et al.*, 1994]; DG, Danish Graben [*Korstgård and Lerche*, 1992]; RG, Rhine Graben [*Weissel and Karner*, 1989]; Tu, Tucano; SeAl, Sergipe-Alagonas [*Karner et al.*, 1992]; EAR, East African Rift [*Ebinger et al.*, 1989]; BK, Baikal [*Ruppel et al.*, 1993]; WNR, White Nile Rift; ARS, African Red Sea; Mom, Mombassa Coast [*Hartley*, 1996]; RoS, Ross Sea [*Stern and ten Brink*, 1989]; Ben, Benue Trough [*Poudjom Djomani et al.*, 1995]; Urals [*Kruse and McNutt*, 1988]; Slave (1.9 Ga) [*Grotzinger and Royden*, 1990]; Slave [*Bechtel et al.*, 1990]; all other points, this study. See text for discussion. The results from the Andes which show a $T_e$ variation of 5 - 85 km are not plotted. This variation reflects the transition from stretched lithosphere (these estimates would plot with those from continental rifts and passive margins) to more cratonic lithosphere. The high values are therefore not a result of strength recovery. We note that $T_e$ in the Slave at 1.9 Ga, a short time after rifting, is much lower than the present-day value, when a long time has elapsed since the rifting event.

1. Forward modeling of gravity anomaly and topography data along closely spaced profiles can be used to recover spatial variations in the long-term elastic thickness $T_e$ of the continental lithosphere.

2. We have found large variations in $T_e$ of the foreland lithosphere at mountain ranges. For the Appalachians, a variation in $T_e$ in the range 40-70 km is found. For the Andes, a variation in the range 5-85 km is found both perpendicular and along strike of the orogen. The foreland lithosphere of the Alps has constant $T_e$ of ~30 km with a weaker zone in the central western Alps ($T_e$ range 5-15 km) increasing toward the eastern Alps.

3. We attribute these variations in $T_e$ to inheritance of the thermal and mechanical properties of foreland lithosphere which has been involved in a cycle of events which began with continental rifting and passive margin formation and ended in continental collision.

4. The pattern of $T_e$ variation observed in the Andes and the requirement for crustal thinning in the Appalachians are consistent with a model in which fold and thrust belts advance across the stretched crust, hinge zone, and coastal plain of former passive margins.

5. Compilations of $T_e$ from continental rifts, passive margins, and foreland lithosphere show large variations. The lowest values are associated with rifts, margins, and foreland lithosphere which has recently been been involved in continental breakup. The highest values are associated with foreland lithosphere where a long time has elapsed since the previous rifting event. We speculate therefore that the stretched continental lithosphere is capable of recovering its strength.

6. The inherited thermal and mechanical structure of the lithosphere may play an important role in influencing the development of the next plate tectonic event.

At mountain ranges, preexisting strength variations offer some control on tectonic style, the geometry of fold and thrust belts, and the stratigraphic patterns that develop in the adjacent foreland basin.

## Appendix: Calculation of Gravity Anomalies and Flexure Modeling

*Parker* [1972] gives an expression for the gravity anomaly measured on the surface $z = z_0$ caused by a layer of anomalous material of density contrast $\Delta\rho$, confined between two surfaces $z_1$ and $z_2$, all functions of position:

$$\mathcal{F}[\Delta g] = -2\pi G e^{-|k|z_0} \sum_{n=1}^{\infty} \frac{(|\,k\,|)^{n-1}}{n!} \mathcal{F}[\Delta\rho(z_1^n - z_2^n)] \tag{A1}$$

where $\mathcal{F}$ represents the Fourier transform of the variable enclosed in brackets and $k$ is the wavenumber. For most rapid convergence, the plane $z = 0$ is best chosen to lie midway between the minimum values of $z_1$ and $z_2$. In practice, the summation involves only the first four terms, and $z_1$ is given by the surface of the undeformed Moho.

The partial differential equation governing the deflection, $w$, of a thin elastic plate of variable thickness overlying an inviscid fluid, adapted from *Timoshenko and Woinowsky-Krieger* [1959], is

$$\begin{aligned}\rho_l g h = {} & D\nabla\nabla w + 2\frac{\partial D}{\partial x}\frac{\partial}{\partial x}\nabla w + 2\frac{\partial D}{\partial y}\frac{\partial}{\partial y}\nabla w + \nabla D\nabla w \\ & - (1-\nu)\left[\frac{\partial^2 D}{\partial x^2}\frac{\partial^2 w}{\partial y^2} - 2\frac{\partial^2 D}{\partial x \partial y}\frac{\partial^2 w}{\partial x \partial y} + \frac{\partial^2 D}{\partial y^2}\frac{\partial^2 w}{\partial x^2}\right] \\ & + (\rho_m - \rho_{in})gw\end{aligned} \tag{A2}$$

where $h$, the load of density $\rho_l$, $\rho_{in}$, the infill density, and $D$ are functions of $x$ and $y$, and $\nabla = (\partial^2/\partial x^2) + (\partial^2/\partial y^2)$. All other parameters are given in Table 1. $D$ is the flexural rigidity given by

$$D(x) = \frac{E T_e(x)^3}{12(1-\nu^2)} \tag{A3}$$

where $E$ and $\nu$ are defined in Table 1.

For the 1-D model equation (A2) depends on $x$ only and reduces to

$$D\frac{d^4 w}{dx^4} + 2\frac{dD}{dx}\frac{d^3 w}{dx^3} + \frac{d^2 D}{dx^2}\frac{d^2 w}{dx^2} + (\rho_m - \rho_{in})gw = \rho_l g h \tag{A4}$$

The boundary conditions for a semi-infinite or broken plate with the break at $x = 0$ are as follows:

1. Zero moment and shear (free edge) at $x = 0$

$$\frac{d^2 w}{dx^2} = 0$$

$$\frac{d^3 w}{dx^3} = 0$$

2. Zero deflection and slope (built-in edge) at $x = \infty$

$$w = 0$$

$$\frac{dw}{dx} = 0$$

Equation (A4) is discretized using standard central difference approximations from *Gahli and Neville* [1989] and the resultant five-band diagonal sparse matrix is solved using a direct LU method [Sparse1.3a, *Kundert and Sangiovanni-Vincentelli*, 1988]. So that boundary condition 2 does not affect the solution, we pad up the topographic load arrays, $h$. It is only possible to test the method for a constant plate thickness where agreement with the analytical solution is to within less than 1%. Many previous 1-D finite difference codes have been based on the code of *Bodine* [1981] which *van Wees and Cloetingh* [1994] state is incorrect. The source of this error appears to be an incorrect expansion of equation (A2) to equation (A4) such that the second term on the left-hand side of equation (A4) is missing. Figure A1 shows the deflection of variable thickness plates due to concentrated vertical forces for this method and *Bodine* [1981]. The solutions agree except when the plate thickness varies very rapidly (approaching a step).

For the 2-D model we follow the approach of *Audet and Watts* [1994] and apply specific boundary conditions to the edges of the plate. Three of the boundaries are free edges, and the fourth edge is a simply supported. These boundary conditions replace the often used condition of zero deflection along all four edges which is geologically unreasonable and affects the solution unless the load is placed well away from the edges. The common solution to this latter problem is to pad the load array (as in the 1-D case) but this rapidly increases computation time. Our boundary conditions overcome this problem.

The boundary conditions of a free edge are zero bending and twisting moment and zero shear. These two boundary conditions, along edges parallel to $x$, are as follows:

1. Twisting moment and shear force are zero

$$\frac{\partial^3 w}{\partial y^3} + (2-\nu)\frac{\partial^3 w}{\partial x^2 \partial y} = 0$$

2. Bending moment is zero

$$\frac{\partial^2 w}{\partial y^2} + \nu\frac{\partial^2 w}{\partial x^2} = 0$$

Similar equations can be written for the free edge parallel to $y$. At the corner between free edges, the twisting moment is zero:

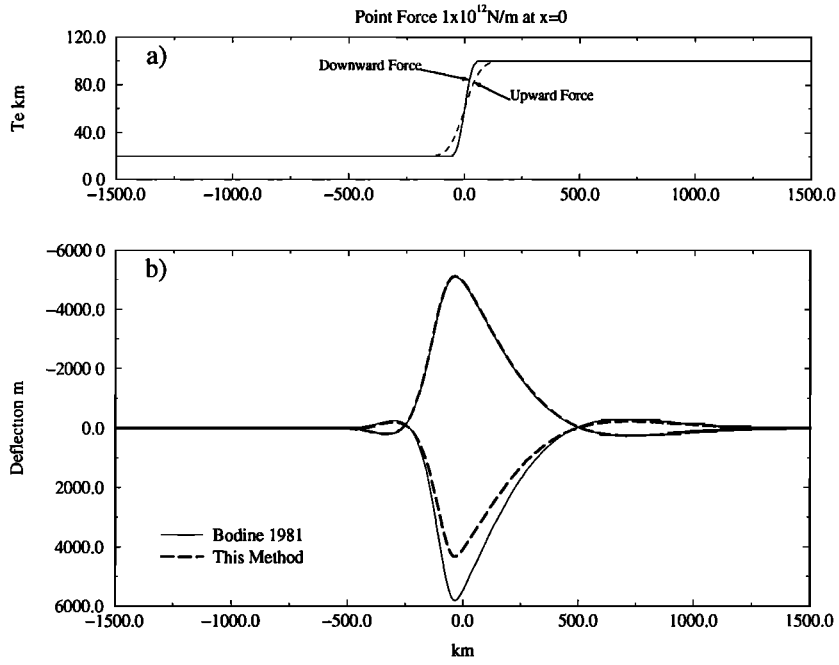


**Figure A1.** Comparison of finite difference methods. (a) $T_e$ structures to which a concentrated force is applied at $x = 0$. (b) Resultant deflections for the method of *Bodine* [1981] (solid) and this method (dashed). Note the significant difference for the downward force on the rapidly varying $T_e$ structure and no difference when the $T_e$ structure is less rapidly varying.

$$\frac{\partial^2 w}{\partial x \partial y} = 0$$

The fourth edge is simply supported and the boundary conditions are as follows:

1. Deflection is zero

$$w = 0$$

2. Bending moment is zero

$$\frac{\partial^2 w}{\partial x^2} = 0$$

A five-band diagonal matrix with fringes results from the discretization of equation (A2), solved using the same software as for the 1-D case. Typical run times for a 100 x 100 grid are 15 min on a Dec Alpha workstation with 128 Mbytes of RAM.

For a grid spacing of 10 km the solution agrees with analytical solutions for constant $T_e$. When the spacing is increased to 20 km, there is a significant decrease in accuracy for low plate thicknesses.

In developing an inverse method for determining the variation of $T_e$ from the observed Bouguer anomaly, we wish to find the most likely model parameters **a** which minimize the misfit between observed and modeled gravity data given by

$$\chi^2 = \sum_{i=1}^{n} \left( \frac{g_i - g(x_i; a_1 \ldots a_M)}{\sigma_i} \right)^2 \qquad \text{(A5)}$$

where $\sigma_i$ are the errors on observed gravity anomalies, which we assume to be unity since we do not know individual errors. The modeled gravity data depend upon the $M$ parameters of **a**. One parameter of **a** is the applied end shear force. The $T_e$ function is constructed from the remaining $M - 1$ parameters by summing the contributions of $M-1$ equally spaced Gaussians of fixed halfwidth of amplitude $a_{i=1-(M-1)}$. Gaussians are used to construct the $T_e$ function because they tend to be more averaging. This is important because, as described above, in solving the flexure problem we must pad up the load arrays. Therefore the $T_e$ function must exist over a greater length than the observed data, and so some of the Gaussians lie in the region of no data and are relatively unconstrained and prone to instability. Splines and polynomials through these points can introduce a spurious effect on that part of the $T_e$ function where data exist and where we want to recover the $T_e$ variation. They are therefore unsuitable for constructing the $T_e$ function. The $\chi^2$ in equation (A5) is minimized using the Levenberg-Marquardt method [*Press et al.*, 1992]. We minimize $\chi^2$ in two stages. First, $\chi^2$ is minimized from the $M$ parameters with the $T_e$ function constructed from $M-1$ Gaussians. Then the number of Gaussians is doubled, and the halfwidth decreased by a factor of two. The best Gaussians amplitudes from the end of the first stage are passed to the nearest two Gaussians at the start of the second stage, and $\chi^2$ for the $2(M-1)+1$ parameters is minimized. Essentially, this is increasing the resolution of the $T_e$ variation.

**Acknowledgments.** We are grateful to J.D. Fairhead at GETECH (University of Leeds) for provision of the SAGP and WEEGP gravity and topography data. Discussions

with S. Lamb, J. Dewey, M. Audet, R. Schegg, and L. Kennan have been useful in formulating the ideas in this paper. C. Stark encouraged J.S. to develop the inverse method and E. Burov, D. Forsyth, and L. Sonder provided helpful and detailed reviews. J.S. acknowledges NERC studentship GT4/94/233/G.

## References

Audet, D. M., and A. B. Watts, Flexure modelling of the northwest African continental margin with an application to the Canary Islands (abstract), *Eos Trans. AGU, 75(44)*, Fall Meet. Suppl., 581, 1994.

Bachmann, G. H., M. Müller, and K. Weggen, Evolution of the Molasse Basin (Germany, Switzerland), *Tectonophysics, 137*, 77–92, 1987.

Barton, P. J., and R. J. Wood, Tectonic evolution of the North Sea Basin: Crustal stretching and subsidence, *Earth Planet. Sci. Lett., 49*, 987–1022, 1984.

Bechtel, T. D., D. W. Forsyth, V. L. Sharpton, and R. A. F. Grieve, Variations in the effective elastic thickness of the North American lithosphere, *Nature, 343*, 636–638, 1990.

Bodine, J. H., Numerical computation of plate flexure in marine geophysics, *Tech. Rep. 1*, Lamont-Doherty Earth Obs., Columbia Univ., Palisades, N.Y., 1981.

Bradley, D. C., and W. S. F. Kidd, Flexural extension of the upper continental crust in collisional foredeeps, *Geol. Soc. Am. Bull., 103*, 1416–1438, 1991.

Brink, H.-J., P. Burri, A. Lunde, and H. Winhard, Hydrocarbon habitat and potential of Swiss and German Molasse Basin: A comparison, *Eclogae Geol. Helv., 85*, 715–732, 1992.

Burov, E. B., and M. Diament, The effective elastic thickness ($T_e$) of continental lithosphere: What does it really mean?, *J. Geophys. Res., 100*, 3905–3927, 1995.

Caporali, A., Gravity anomalies and the flexure of the lithosphere in the Karakoram, Pakistan, *J. Geophys. Res., 100*, 15075–15085, 1995.

Chigne, N., and L. Hernandez, Main aspects of petroleum exploration in the Apure area of Southwestern Venezuela 1985-1988, in *Classic Petroleum Provinces*, edited by J. Brooks, *Geol. Soc. Spec. Publ. 50*, 55–75, 1990.

Cloetingth, S., and E. B. Burov, Thermomechanical structure of European continental lithosphere: constraints from rheological profiles and EET estimates, *Geophys. J. Int., 124*, 695–723, 1996.

Cook, F. A., and J. E. Oliver, The late Precambrian-early Paleozoic continental edge in the Appalachian orogen, *Am. J. Sci., 281*, 993–1008, 1981.

Dewey, J. F., Plate tectonics and the evolution of the British Isles, *J. Geol. Soc. London, 139*, 371–412, 1982.

Diament, M., J. C. Sibuet, and A. Hadaqui, Isostasy of the northern Bay of Biscay continental margin, *Geophys. J. R. Astron. Soc., 86*, 893–907, 1986.

Diecchio, R. J., Stratigraphic interpretation of the Ordovician of the Appalachian basin and implications for Taconian flexural modeling, *Tectonics, 12*, 1410–1419, 1993.

Dorman, L. M., and B. T. R. Lewis, Experimental isostasy, 1, Theory of determination of the Earth's isostatic response to a concentrated load, *J. Geophys. Res., 75*, 3357–3365, 1970.

Ebinger, C. J., T. D. Bechtel, D. W. Forsyth, and C. O. Bowin, Effective elastic plate thickness beneath the East African and Afar Plateaus and dynamic compensation of the uplifts, *J. Geophys. Res., 94*, 2883–2901, 1989.

Forsyth, D. W., Subsurface loading and estimates of the flexural rigidity of continental lithosphere, *J. Geophys. Res., 90*, 12623–12632, 1985.

Fowler, S., and D. P. McKenzie, Gravity studies of the Rockall and Exmouth Plateaus using Seasat altimetry, *Basin Res., 2*, 27–34, 1989.

Gahli, A., and A. M. Neville, *Structural Analysis: A Unified Classical and Matrix Approach*, 3rd ed., Chapman and Hall, New York, 1989.

Green, C. M., and J. D. Fairhead, The South American Gravity Project, in *Recent Geodetic and Gravimetric Research in Latin America*, edited by W. Torge, A. Fletcher, and J. Tanner, pp. 82–95, Springer-Verlag, New York, 1991.

Grotzinger, J., and L. Royden, Elastic thickness of the Slave Craton at 1.9 Gyr and implications for the thermal evolution of the continents, *Nature, 347*, 64–66, 1990.

Gutscher, M.-A., Crustal structure and dynamics in the Rhine Graben and the Alpine foreland, *Geophys. J. Int., 122*, 617–636, 1995.

Haq, B. U., J. Hardenbol, and P. R. Vail, Chronology of fluctuating sea-levels since the Triassic, *Science, 235*, 1156–1167, 1987.

Hartley, R. W., Isostasy of Africa: Implications for the thermo-mechanical behaviour of the continental lithosphere, Ph.D. thesis, Univ. of Oxford, Oxford, England, 1996.

Hartley, R. W., A. B. Watts, and J. D. Fairhead, Isostasy of Africa, *Earth Planet. Sci. Lett., 137*, 1–18, 1996.

Hatcher, R. D., Jr., Tectonic synthesis of the U.S. Appalachians, in vol. F2, *The Geology of North America, The Appalachian-Ouachita Orogen in the United States*, edited by R. D. Hatcher Jr., W. A. Thomas, and G. W. Viele, pp. 511–535, Geol. Soc. of Am., Boulder, Colo., 1989.

Holt, W. E., and T. A. Stern, Sediment loading on the Western Platform of the New Zealand continent, *Earth Planet. Sci. Lett., 107*, 523–538, 1991.

Hutchinson, D. R., J. A. Grow, and K. D. Klitgord, Crustal structure beneath the southern Appalachians: Nonuniqueness of gravity modeling, *Geology, 11*, 661–615, 1983.

Janssen, M. E., M. Torné, S. Cloetingh, and E. Banda, Pliocene uplift of the eastern Iberian margin: Inferences from quantitative modelling of the Valencia Trough, *Earth Planet. Sci. Lett., 119*, 585–597, 1993.

Judge, A. V., and M. K. McNutt, The relationship between plate curvature and elastic plate thickness: A study of the Peru-Chile Trench, *J. Geophys. Res., 96*, 16625–16640, 1991.

Karner, G., S. Egan, and J. Weissel, Modeling the tectonic development of the Tucano and Sergipe-Alagonas rift basins, Brazil, *Tectonophysics, 215*, 133–160, 1992.

Karner, G. D., and A. B. Watts, On isostasy at Atlantic-type continental margins, *J. Geophys. Res., 87*, 2923–2948, 1982.

Karner, G. D., and A. B. Watts, Gravity anomalies and flexure of the lithosphere at mountain ranges, *J. Geophys. Res., 88*, 10449–10477, 1983.

Kaula, W. M., Earth's gravity field: Relation to global tectonics, *Science, 169*, 982–985, 1969.

Kooi, H., S. Cloetingh, and J. Burrus, Lithospheric necking and regional isostasy at extensional basins, 1, Subsidence and gravity modeling with an application to the Gulf of Lions Margin (SE France), *J. Geophys. Res., 97*, 17553–17571, 1992.

Korstgård, J. A., and I. Lerche, Flexural plate reprensentation of Danish Central Graben evolution, *J. Geodyn., 16*, 181–209, 1992.

Kruse, S., and M. K. McNutt, Compensation of Paleozoic orogens: A comparison of the Urals to the Applachians, *Tectonophysics, 154*, 1–17, 1988.

Kundert, K. S., and A. Sangiovanni-Vincentelli, *Sparse*

*User's Guide*, Version 1.3a, Dep. of Electr. Eng. and Comput. Sci., Univ. of Calif., Berkeley, 1988.

Kusznir, N. J., G. Marsden, and S. S. Egan, A flexural-cantilever simple-shear/pure-shear model of continental lithosphere extension: Applications to the Jeanne d'Arc Basin, Grand Banks and Viking Graben, North Sea, in *The Geometry of Normal Faults*, edited by A. M. Roberts, G. Yielding, and B. Freeman, *Geol. Soc. Spec. Publ. 56*, 41–60, 1991.

Lowry, A. R., and R. B. Smith, Flexural rigidity of the Basin and Range-Colorado Plateau-Rocky Mountain transition from coherence analysis of gravity and topography, *J. Geophys. Res.*, *99*, 20123–20140, 1994.

Lyon-Caen, H., and P. Molnar, Constraints on the structure of the Himalaya from an analysis of gravity anomalies and a flexural model of the lithosphere, *J. Geophys. Res.*, *88*, 8171–8191, 1983.

Macario, A., A. Malinverno, and W. F. Haxby, On the robustness of elastic thickness estimates obtained using the coherence method, *J. Geophys. Res.*, *100*, 15163–15172, 1995.

Magnavita, L. P., I. Davison, and N. J. Kusznir, Rifting, erosion, and uplift history of the Recôncavo-Tucano-Jatobá Rift, northeast Brazil, *Tectonics*, *13*, 367–388, 1994.

McNutt, M. K., and R. L. Parker, Isostasy of Australia and the evoloution of the compensation mechanism, *Science*, *199*, 773–775, 1978.

McNutt, M. K., M. Diament, and M. G. Kogan, Variations of elastic plate thickness at continental thrust belts, *J. Geophys. Res.*, *93*, 8825–8838, 1988.

Milici, R. C., and W. de Witt Jr., The Appalachian Basin, in vol. D2, *The Geology of North America*, *Sedimentary Cover-North American Craton*, edited by L. L. Sloss, pp. 427–469, Geol. Soc. of Am., Boulder, Colo., 1988.

Nunn, J. A., M. Czerniak, and R. H. Pilger, Constraints on the structure of the Brooks Range and Colville Basin, northern Alaska, from flexure and gravity analysis, *Tectonics*, *6*, 603–617, 1987.

Parker, R. L., The rapid calculation of potential anomalies, *Geophys. J. R. Astron. Soc.*, *31*, 447–445, 1972.

Pfiffer, O. A., and P. F. Erard, Two cross sections through the Swiss Molasse Basin, in *Deep Structure of the Swiss Alps: Results from NFP/PNR 20*, edited by O. A. Pfiffer, A. Steck, P. Heitzmann, and P. Lehner, Birkhäuser, Basel, in press, 1996.

Pitcher, W. S., M. P. Atherton, E. J. Cobbing, and R. D. Beckinsale, *Magmatism at a Plate Edge: The Peruvian Andes*, John Wiley, New York, 1985.

Poudjom Djomani, Y. H., J. M. Nnange, M. Diament, C. J. Ebinger, and J. D. Fairhead, Effective elastic thickness and crustal thickness variations in west central Africa inferred from gravity data, *J. Geophys. Res.*, *100*, 22047–22070, 1995.

Press, W. H., B. P. Flannery, S. A. Teukoslsky, and W. T. Vetterling, *Numerical Recipes in C*, 2nd ed., Cambridge Univ. Press, New York, 1992.

Quinlan, G. M., and C. Beaumont, Appalachian thrusting, lithospheric flexure, and the Paleozoic stratigraphy of the eastern interior of North America, *Can. J. Earth Sci.*, *21*, 973–996, 1984.

Rapp, R. H., Y. M. Wang, and N. K. Pavlis, The Ohio State 1991 geopotential and sea surface topography harmonic coefficient models, *Tech. Rep. 410*, Dep. of Geod. Sci. and Surv., Ohio State Univ., Columbus, 1991.

Royden, L. H., and F. Horváth (Eds.), *The Pannonian Basin: A Study in Basin Evolution*, *AAPG Mem.*, *45*, 1988.

Royden, L. H., and G. D. Karner, Flexure of the lithosphere beneath the Apennine and Carpathian foredeep: Evidence for an insufficient topographic load, *AAPG Bull.*, *68*, 704–712, 1984.

Ruppel, C., M. G. Kogan, and M. K. McNutt, Implications of new gravity data for Baikal rift zone structure, *Geophys. Res. Lett.*, *20*, 1635–1638, 1993.

Schegg, R., W. Leu, C. Cornford, and P. A. Allen, New coalification profiles in the Swiss Molasse Basin (Western Switzerland): Implications for the thermal and geodynamic evolution of the Alpine foreland, *Eclogae Geol. Helv.*, *90*, in press, 1997.

Sinclair, H. D., B. J. Coakley, P. A. Allen, and A. B. Watts, Simulation of foreland basin stratigraphy using a diffusion model of mountain belt uplift and erosion: An example from the central Alps, Switzerland, *Tectonics*, *10*, 599–620, 1991.

Smith, W. H. F., and P. Wessel, Gridding with continuous curvature splines in tension, *Geophysics*, *55*, 293–305, 1990.

Spadini, G., S. Cloetingh, and G. Bertotti, Thermomechanical modeling of the Tyrrhenian Sea: Lithospheric necking and kinematics of rifting, *Tectonics*, *14*, 629–644, 1995.

Stern, T. A., and U. S. ten Brink, Flexural uplift of the Transantarctic Mountains, *J. Geophys. Res.*, *94*, 10315–10330, 1989.

Stockmal, G. S., C. Beaumont, and R. Boutilier, Geodynamic models of convergent margin tectonics: Transition from rifted margin to overthrust belt and consequences for foreland basin development, *AAPG Bull.*, *70*, 181–190, 1986.

Tankard, A. J., On the depositional response to thrusting and lithospheric flexure: examples from the Appalachian and Rocky Mountain basins, in *Foreland Basins*, edited by P. A. Allen and P. Homewood, *Spec. Publ. Int. Assoc. Sedimentol.*, *8*, 369–392, 1986.

Taylor, P. T., and D. Ravat, An interpretation of the Magsat anomalies of central Europe, *J. Appl. Geophys.*, *34*, 83–91, 1995.

Taylor, S. R., Geophysical framework of the Appalachians and adjacent Grenville Province, in *Geophysical Framework of the Continental United States*, edited by L. C. Pakiser and W. D. Mooney, *Mem. Geol. Soc. Am. 172*, 317–348, 1989.

Thomas, W. A., The Appalachian-Ouachita rifted margin of southeastern North America, *Geol. Soc. Am. Bull.*, *103*, 415–431, 1991.

Timoshenko, S. P., and S. Woinowsky-Krieger, *Theory of Plates and Shells*, 2nd ed., McGraw-Hill, New York, 1959.

Toth, J., N. J. Kusznir, and S. S. Flint, A flexural isostatic model of lithosphere shortening and foreland basin formation: Application to the Eastern Cordillera and Subandean belt of NW Argentina, *Tectonics*, *15*, 213–223, 1996.

Vail, P. R., R. M. Mitchum, Jr., R. G. Todd, J. M. Widmier, S. Thompson, III., J. B. Sangree, J. N. Bubb, and W. G. Hatleilid, Seismic stratigraphy and global changes of sea level, in *Seismic Stratigraphy-Applications to Hydrocarbon Exploration*, edited by C. E. Payton, *Mem. Am. Assoc. Pet. Geol, 26*, 49–212, 1977.

van Wees, J. D., and S. Cloetingh, A finite-difference technique to incorporate spatial variations in rigidity and planar faults into 3-D models for lithospheric flexure, *Geophys. J. Int.*, *117*, 179–195, 1994.

Walcott, R. I., Flexure of the lithosphere at Hawaii, *Tectonophysics*, *9*, 435–446, 1970.

Ward, L. W., and G. L. Strickland, Outline of Tertiary stratigraphy and depositional history of the U.S. Atlantic coastal plain, in *Geological Evolution of the United States Atlantic Margin*, edited by C. Poag, pp. 87–123, Van Nostrand Rheinhold, New York, 1985.

Waschbusch, P. J., and L. H. Royden, Spatial and temporal evolution of foredeep basins: Lateral strength variations and inelastic yielding in continental lithosphere, *Basin Res.*, *4*, 179–196, 1992.

Watts, A. B., An analysis of isostasy in the world's oceans, 1, Hawaiian-Emperor seamount chain, *J. Geophys. Res.*, *83*, 5989–6004, 1978.

Watts, A. B., Gravity anomalies, crustal structure and flexure of the lithosphere at the Baltimore Canyon Trough, *Earth Planet. Sci. Lett.*, *89*, 221–238, 1988.

Watts, A. B., The effective elastic thickness of the lithosphere and the evolution of foreland basins, *Basin Res.*, *4*, 169–178, 1992.

Watts, A. B., and J. R. Cochran, Gravity anomalies and flexure of the lithospere along the Hawaiian-Emperor Seamount Chain, *Geophys. J. R. Astron. Soc.*, *38*, 119–141, 1974.

Watts, A. B., and M. Torné, Crustal structure and the mechanical properties of extended continental lithosphere in the Valencia Trough (western Mediterranean), *J. Geol. Soc. London*, *149*, 813–827, 1992.

Watts, A. B., S. H. Lamb, J. D. Fairhead, and J. F. Dewey, Lithospheric flexure and bending of the Central Andes, *Earth Planet. Sci. Lett.*, *134*, 9–21, 1995.

Weissel, J. K., and G. D. Karner, Flexural uplift of rift flanks due to mechanical unloading of the lithosphere during extension, *J. Geophys. Res.*, *94*, 13919–13950, 1989.

Wessel, P., A reexamination of the flexural deformation beneath the Hawaiian islands, *J. Geophys. Res.*, *98*, 12177–12190, 1993.

Wessel, P., and A. B. Watts, On the accuracy of marine gravity measurements, *J. Geophys. Res.*, *93*, 393–413, 1988.

Whitman, D., Moho geometry beneath the eastern margin of the Andes, northwest Argentina, and its implications to the effective elastic thickness of the Andean foreland, *J. Geophys. Res.*, *99*, 15277–15289, 1994.

Zoetemeijer, R., P. Desegaulx, S. Cloetingh, F. Roure, and I. Moretti, Lithospheric dynamics and tectonic-stratigraphic evolution of the Ebro Basin, *J. Geophys. Res.*, *95*, 2701–2711, 1990.

Zuber, M. T., T. D. Bechtel, and D. W. Forsyth, Effective elastic thickness of the lithosphere and mechanisms of isostatic compensation in Australia, *J. Geophys. Res.*, *94*, 9353–9367, 1989.

J. Stewart and A.B. Watts, Department of Earth Sciences, Oxford University, Parks Road, Oxford OX1 3PR, England. (e-mail: jons@earth.ox.ac.uk; tony@earth.ox.ac.uk)

(Received May 20, 1996; revised November 15, 1996; accepted November 21, 1996.)